Regenerative Biomaterials, 2021, 1–20
doi: 10.1093/rb/rbab047
Advance Access Publication Date: 12 August 2021
Research Article

OXFORD

Integrated printed BDNF/collagen/chitosan scaffolds with low temperature extrusion 3D printer accelerated neural regeneration after spinal cord injury

Xiao-Yin Liu[1,2,3,4,†], Chong Chen[1,2,†], Hai-Huan Xu[1,2,†], Yu-sheng Zhang[3], Lin Zhong[5], Nan Hu[1], Xiao-Li Jia[1], You-Wei Wang[1], Kun-Hong Zhong[4], Chang Liu[4], Xu Zhu[2], Dong Ming[1,*] and Xiao-Hong Li[1,*]

[1]Tianjin Key Laboratory of Brain Science and Neural Engineering, Academy of Medical Engineering and Translational Medicine, Tianjin University, Tianjin 300072, China; [2]Tianjin Key Laboratory of Neurotrauma Repair, Pingjin Hospital Brain Center, Characteristic Medical Center of PAPF, Tianjin 300162, China; [3]National Engineering Research Center in Biomaterials, College of Biomedical Engineering, Sichuan University, Chengdu 610064, Sichuan, China; [4]Department of Neurosurgery, West China Medical School, West China Hospital, Sichuan University, Chengdu 610041, Sichuan, China; and [5]Department of Hematology, The First Affiliated Hospital of Chengdu Medical College, Chengdu 610500, Sichuan, China

[†]These authors contributed equally to this study.

*Correspondence address. Tianjin Key Laboratory of Brain Science and Neural Engineering, Academy of Medical Engineering and Translational Medicine, Tianjin University, Tianjin 300072, China. Tel: +86-022-83612122; Fax: +86-022-83612122; E-mail: lixiaohong12@hotmail.com; richardming@tju.edu.cn

Received 16 March 2021; revised 19 July 2021; accepted on 1 August 2021

Abstract

Recent studies have shown that 3D printed scaffolds integrated with growth factors can guide the growth of neurites and promote axon regeneration at the injury site. However, heat, organic solvents or cross-linking agents used in conventional 3D printing reduce the biological activity of growth factors. Low temperature 3D printing can incorporate growth factors into the scaffold and maintain their biological activity. In this study, we developed a collagen/chitosan scaffold integrated with brain-derived neurotrophic factor (3D-CC-BDNF) by low temperature extrusion 3D printing as a new type of artificial controlled release system, which could prolong the release of BDNF for the treatment of spinal cord injury (SCI). Eight weeks after the implantation of scaffolds in the transected lesion of T10 of the spinal cord, 3D-CC-BDNF significantly ameliorate locomotor function of the rats. Consistent with the recovery of locomotor function, 3D-CC-BDNF treatment could fill the gap, facilitate nerve fiber regeneration, accelerate the establishment of synaptic connections and enhance remyelination at the injury site.

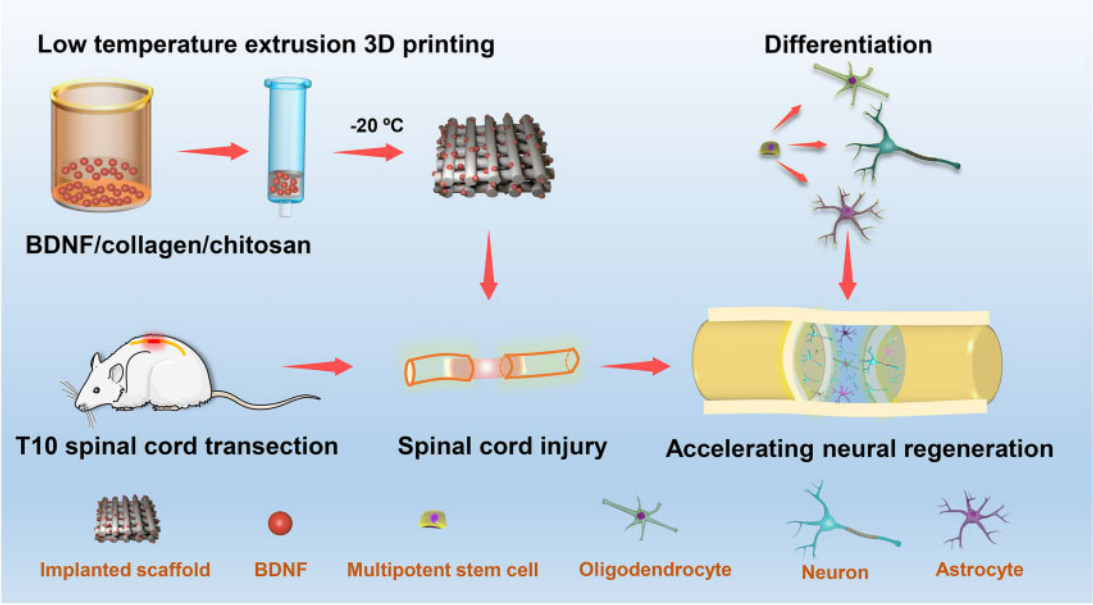

Keywords: low temperature extrusion 3D printing; brain-derived neurotrophic factor; collagen; chitosan; diffusion tensor imaging; spinal cord injury

Introduction

Spinal cord injury (SCI), a serious trauma of the central nervous system, is characterized by high morbidity and high disability rate [1]. The factors causing disability after SCI include axonal degeneration, losing of neurons, abnormal activation of immune cells, etc. A cascade of pathological processes occurs after SCI, which includes inflammation, edema, ischemia, infiltration of immune cells, lipid peroxidation, axon loss, cystic cavity, and glial scarring, forming an adverse environment that causes limited regeneration of axons [2–5]. Therefore, nerve repair after SCI is still a challenging clinical problem [6]. Recent research tried to create a proper environment for axonal regeneration by providing natural or synthetic scaffold to guide the axon growth to the correct direction. 3D printed scaffolds combine with growth factors have been widely used to reconnect with the area of the SCI [7, 8]. However, the 3D printing technique using high temperature or aggressive chemicals impairs the biological activity of growth factors, because growth factors lose their biological activity at temperatures higher than body temperature, or are denatured by chemicals. In our study, the low temperature 3D printing incorporated growth factors into the scaffold and maintained the biological activity of growth factors during printing [9, 10].

The scaffolds require not only good mechanical properties, but also porosity to provide a microenvironment for spinal axonal regeneration [11]. Traditional scaffolds preparation technology, such as freeze-drying, particulate leaching, organic foam impregnation and pore-forming agent [12], fail to form a fixed morphology and regular scaffold structure. 3D printing is an emerging technique for making biological scaffolds using digital modeling and imaging techniques based on computer-aided planning and 3D design. Through the 3D printing technology, the mechanical properties of the scaffolds can be regulated by designing the structure, and the biological activity and degradation of the scaffolds can be adjusted by chemical composition [10, 13]. 3D printing technology can produce spinal bionic scaffolds with appropriate structure, size and shape to achieve individualized scaffold [14, 15]. 3D bioprinting technology is a branch and extension of 3D printing technology, which is a combination of additive manufacturing and cell printing, and is the product of technology integration in different fields such as engineering, biomaterials, cell biology, physics, chemistry, manufacturing and medicine. 3D bioprinting technology is an emerging, rapidly expanding, vigorous and most promising technology field in 3D printing technology. It is considered to be a new paradigm of tissue engineering and biomanufacturing in the 21st century, and has been increasingly used in tissue engineering [16, 17].

Three main types of bioprinting technologies are commonly used, namely micro-extrusion molding, inkjet and laser-assisted bioprinting technology (LAB). LAB, also known as laser bioprinting technology, uses laser energy to promote the formation of scaffolds materials. However, the time required for LAB to print the scaffolds is relatively long, and the new biomaterials that need to form a cross-linking reaction are difficult to obtain, which further limits the clinical application of LAB. Although LAB can pinpoint the location of cells in a material, its ability to construct a scaffold in the vertical direction is highly limited. Inkjet bioprinting technology is ideal for accurate printing of cells and biomaterials, which uses 2D inkjet printing layers to build 3D structural scaffolds [18]. However, inkjet printing technology has a high time requirement for gel formation of biological materials, which limits the selection of suitable biomaterials. During the printing process, the biomaterial is extruded through a nozzle onto a substrate by extrusion printing techniques to create a pre-designed structure. Unlike inkjet bioprinting, extrusion bioprinting uses high-viscosity materials, which allowed engineers to make scaffolds from a variety of biomaterials. Although the printing speed is not as fast as that of inkjet bioprinting, extrusion bioprinting is easier to print growth factors or cells [19]. Extrusion bioprinting technology re-arranges biomaterials containing neurotrophic factor or cells using pressure or screw extrusion. Today, micro-

extrusion bioprinting technology has become one of the most economical rapid prototyping technologies, but the harmful effects of shear forces on cell viability and polymerization during printing must be carefully considered. Compared to other methods, extrusion bioprinting technology can quickly print out the scaffold material and form a complex physical structure, while also accelerate the formation of biomaterials with high growth factor and cell concentrations. The use of modified biocompatible materials during printing can effectively increase the viability of growth factors and cells. Extrusion molding technology is a kind of additive manufacturing technology, the principle of which is to extrude biological materials from the nozzle, layer by layer drawing superposition to form an object [20]. The principle of extrusion through a nozzle enables the printing process to be carried out at low temperatures, which is different from the principle of melt deposition manufacturing technology which uses high temperature molten material to print. This advantage makes it possible to add bioactive factors to the raw material, and the low temperature process can retain the bioactive factors to the maximum extent.

Many rigid materials have poor biocompatibility, slow degradation, immunogenicity, or tumorigenicity. Implanting these rigid materials into the central nervous system may produce immune response, inflammatory response, cytotoxic response and tumor. Due to the soft tissue characteristics of the spinal cord, biomaterials with mechanical properties close to the spinal cord tissue are often selected as biomaterials for scaffolds for SCI treatment. Collagen material is a common natural polymer, which is often used to make scaffolds because of biodegradability, biocompatibility, abundance and low immunogenicity. However, collagen has the disadvantage of rapid degradation and poor mechanical strength, which prevents it from becoming good scaffold materials for SCI [21]. Chitosan has biodegradability, low toxicity and good ductility, which has often been used to promote the nerve repair to enable functional recovery after SCI [22, 23]. Chitosan has often been used as a scaffold carrier, which can control growth factors release and extend the effect of growth factors [24]. Adding chitosan to collagen can delay the degradation of collagen. Chitosan can also increase the mechanical strength of the collagen scaffold, so the collagen chitosan scaffold is an ideal scaffold for the treatment of SCI.

Growth factors are critical for nerve regeneration. Conventional 3D bioprinting molds the scaffolds before the growth factors adhere to the established scaffolds. In this case, the adhesion of the growth factors to the scaffold is not tight and homogenous sufficiently, often resulting in insufficient or uncontrolled releasing process. The 3D integrated printed scaffolds and growth factors could promote the growth factors adherering to the scaffold more tightly and more uniformly, which makes the robust and stable growth factor releasing from the scaffold.

The manufacturing process of scaffolds usually involved high temperature or laser sintering, which caused damage to the incorporated growth factors [25]. The low temperature 3D printing technology can avoid the requirement of the photosensitive material by the laser curing forming technology, and can also avoid the influence of the high temperature environment of the melting process on the biological activity of the material and the growth factor, which is expected to solve a series of problems in the conventional scaffold preparation method. Low temperature 3D printing can maintain the biological activity of growth factors. Brain-derived neurotrophic factor (BDNF) plays a vital role in the development of nervous system and has neuroprotective effects on various neurons after injury [26, 27]. Previous studies showed that through activation of Tyrosine Kinase receptor B (TrkB), BDNF promoted axonal regeneration and functional recovery after SCI [28–30]. Nevertheless, the rapid diffusion and short half-life in scaffolds impaired the biological function of BDNF for neuron protection and regeneration. Different with other scaffold preparation techniques, extrusion 3D printing can prepare scaffolds at low temperatures, making it possible to incorporate growth factors into the scaffolds and also maintain biological activity.

In the current studies, we prepared collagen/chitosan scaffolds integrated with brain-derived neurotrophic factor (3D-CC-BDNF) by low temperature extrusion 3D printing as a new type of controlled system that could prolong the release of BDNF. The role of 3D-CC-BDNF in bridging the injured area and ameliorating functional recovery after SCI.

Materials and methods

Fabrication of scaffolds

Collagen/chitosan compound material, including 6 g collagen I and 3 g chitosan (deacetylation degree 75–85%, Sigma, St. Louis, USA) was prepared as previously described [13, 31]. Briefly, sterile compound material was incubated at 4°C overnight. BDNF protein solution (Sigma, St. Louis, USA) was sterilized by using a 0.22 μm filter (Millipore, Massachusetts, USA) at 4°C. Then to equilibrium binding, half of sterile collagen–chitosan compound material were soaked with 20 μl of 0.05 mg/ml BDNF solution and incubated for 24 h at 4°C. After stirring at 4°C for 12 h, the mixed solution was incubated at 4°C overnight. Constructs were prepared by a 3D printer (Regenovo, Hangzhou, China) at −20°C. The printing parameters were as follows: platform temperature = −20°C, nozzle diameter = 160 μm, extrusion speed = 0.17 mm/min, printing speed = 12 mm/s, thickness = 0.3 mm per layer. The prepared mixed solution (collagen/chitosan compound material or collagen/chitosan compound material combined with BDNF) was placed in printer cartridge. After printing, the 3D solid molding (3D printed collagen/chitosan scaffold (3D-CC)) and 3D printed collagen/chitosan scaffold integrated with BDNF (3D-CC-BDNF)) was stored at −80°C overnight followed by vacuum cooling and drying for 48–72 h. 3D-CC and 3D-CC-BDNF were made into 2 mm × 3 mm × 3 mm cylinder by using a hole punch. 3D-CC was soaked in 20 μl of 0.05 mg/ml BDNF solution for 24 h at 4°C to fabricate 3D printed collagen/chitosan scaffold adsorbed with BDNF (3D-CC + BDNF). All scaffolds were sterilized with ^{60}Co at 4°C and washed for 30 min by D-Hank's. There were six different scaffolds in this study: collagen scaffold adsorbed with BDNF (the C + BDNF group), collagen/chitosan adsorbed with BDNF (the CC + BDNF group), 3D printed collagen scaffold adsorbed with BDNF (the 3D-C + BDNF group), 3D printed collagen/chitosan scaffold adsorbed with BDNF (the 3D-CC + BDNF group), 3D printed collagen scaffold integrated with BDNF (the 3D-C-BDNF group), and 3D printed collagen/chitosan scaffold integrated with BDNF (the 3D-CC-BDNF group). All scaffolds fabrication processes were performed sterilely and at a low temperature of 4°C to maintain the activity of BDNF [32].

In vivo degradation test of scaffolds

Twenty female Sprague-Dawley (SD) rats (about 300 g) were selected. To explore the suitable mass ratio scaffold used in this study, 3D-CC-BDNF scaffolds with five kinds of mass ratio were fabricated (collagen: chitosan = 1:5, 1:2, 1:1, 2:1, 5:1). The *in vivo* degradation experiments of the scaffolds were carried out according to

established methods [33]. Briefly, after anesthesia, the backs of all rats were cut to form three small openings about 1 cm long. Three sterile scaffolds of the same mass ratio were placed into three dorsal incisions of rats ($n = 3$). 2, 4, 6 and 8 weeks after the surgery, scaffolds with five kinds of mass were removed from the back of the rats to assess *in vivo* degradation behavior. To completely decellularize the scaffolds, the scaffolds were soaked in DNase–RNase I digestion solution (Solarbio Science & Technology Co., Ltd, China). Percent mass remaining = (decellularized scaffold mass/initial mass) × 100%. The details of the number of rats used in the experiment were shown in Supplementary Table S1.

Physical properties measurement

The gravimetric method was used to measure the water absorption ratio of the scaffolds, and the volume method was used performed to measure the porosity ratio [34]. Instron 5865 mechanical tester was performed to test compressive mechanical properties. The preload 0.05 N, maximum compressive strain was 30%. Each sample was tested three times for the stress–strain curve. The elastic modulus of scaffolds was calculated to analyze the mechanical properties. To measure the stability of the 3D-CC-BDNF and BDNF protein (control), differential scanning calorimetry (DSC) was performed by the Synchronous Differential Thermal Analyzer (STA409PC/PG, Germany). The FTIR-ATR spectrum of 3D-CC+BDNF and 3D-CC-BDNF was analyzed by using an FTIR spectrometer (VERTEX, Bruker, Germany) [35].

Determination of kinetics of BDNF release from 3D-CC-BDNF

Scaffolds were placed in PBS at 37°C. The supernatants were collected at 1, 3, 5, 7, 12, 21 and 28 days after incubation. Fresh PBS was then used to completely replace the supernatants. The amount of BDNF in the supernatants at each time interval was analyzed by enzyme-linked immunosorbent assay (BDNF Immunoassay, R&D Systems®, USA).

In vivo test of BDNF release from the scaffold

In brief, the rats were randomly divided into two groups (55 rats per group). After the rat was anesthetized, SCI model was established. 3D-CC-BDNF and 3D-CC+BDNF were both implanted into the gap, respectively. Spinal cords of rats were obtained at 1, 7, 14, 21 and 28 days after implantation. Enzyme-linked immunosorbent assay (ELISA, R&D Systems, Minneapolis, Minnesota, USA) was subsequently used to quantify BDNF. Four rats died during the surgery (3D-CC+BDNF group: 2, 3D-CC+BDNF group: 2). Four rats died due to bacterial infection within 28 days after SCI (3D-CC+BDNF: 3, 3D-CC-BDNF group: 1). The details of the number of rats used in the experiment were shown in Supplementary Table S2.

Cell culture

Neural stem cells (NSCs) were isolated from embryonic day 14 (E14) brains and cultured according to established methods [36]. Immunofluorescence staining for Nestin (1:500, Abcam, Cambridge, UK) was performed to identify NSCs. Human umbilical cord mesenchymal stem cells (HUCMSCs) were isolated from healthy newborn umbilical cords [37, 38]. HUCMSCs were identified by flow cytometry according to existing methods [37, 38]. Flow cytometry was used to analyze the expression of CD90, CD105, CD73, CD116, CD19, CD45 and HLA-DR (Abcam Cambridge, UK) on HUCMSCs. Immunofluorescence was performed to detect the expression of CD90 (1:300, Abcam, Cambridge, UK) and CD105 (1:400, Abcam, Cambridge, UK)) in HUCMSCs. NSCs or HUCMSCs at the fourth generation were used in the subsequent assays. NSCs or HUCMSCs were inoculated at a density of 1×10^6/ml into the scaffold. At 7 days after the initiation of co-culture, the number of cells, the length of cell protrusions and angle of cell protrusions were assessed by an inverted phase contrast microscope (Nikon, Tokyo, Japan). After 7 days of incubation with NSCs or HUCMSCs and scaffolds, cell morphology and growth were evaluated by scanning electron microscope (SEM) (Hitachi, Tokyo, Japan). At 7 days after co-culture of NSCs or HUCMSCs with the scaffold, the cell–scaffold complex was subjected to hematoxylin–eosin (HE) staining. After co-culture of HUCMSCs with the scaffold for 7 days, immunofluorescence staining was carried out to detect HUCMSCs in 3D-CC-BDNF or 3D-CC+BDNF under a fluorescent microscope (Leica TCS SP5, DMI400B, Leica, Germany). To measure cell adhesion rate, the scaffold was placed in a 96-well plate. 20 µl of NSCs single cell suspension was seeded on a scaffold at a concentration of 5×10^6/ml. At 1, 6, 12, 24, 48 and 96 h after seeding, cell adhesion rate of NSCs was calculated as follows: cell adhesion rate = (number of adherent cells/number of seeding cells) × 100%. The viability of NSCs or HUCMSCs during co-culture was evaluated by using CCK-8 assay (Sigma-Aldrich, St. Louis, MO, USA). The obtained neurospheres were seeded with three kinds of media: I, the medium plus 3D-CC (10 mg/ml 3D-CC without BDNF); II, the medium plus the 3D-CC+BDNF (the 10 mg/ml 3D-CC combined with 20 ng BDNF); III, the medium plus the 3D-CC-BDNF (10 mg/ml 3D-CC integrated with 20 ng BDNF). At 7 days and 2 weeks after co-culture, immunofluorescence staining was used to evaluate the morphology of the NSCs.

SCI model and scaffold transplantation

All animal experimental protocols were implemented according to 'Policies on the Use of Animals and Humans in Neuroscience Research' and were approved by the Institutional Animal Care and Use Committee of Logistics University of People's Armed Police (PAP) (approval No. 2018-0023.7). Our study was not preregistered.

Adult female SD rats (220-250 g) were anesthetized through intraperitoneal injection of 1% pentobarbital sodium (40 mg/kg). Following laminectomy at T8–T12 by using bone rongeur forceps, a 2.0 mm gap in the spinal cord of T10 was created by completely removing the 2.0 mm spinal cord segment at T10 with an angled microscissor. After complete hemostasis, the scaffolds were embedded into the transected gap. All rats were randomly assigned into four groups: Sham group (only laminectomy without SCI, $n = 30$), SCI group (SCI without transplantation, $n = 30$), 3D-CC+BDNF group (3D-CC+BDNF was implanted into completely-transected gap, $n = 30$) and 3D-CC-BDNF group (3D-CC-BDNF was implanted into completely-transected gap, $n = 30$). Two rats in the injury group died during the operation (SCI group: 1, 3D-CC-BDNF group: 1). Within 8 weeks after SCI, five rats in the injury group died due to bacterial infection (SCI group: 2, 3D-CC+BDNF: 2, 3D-CC-BDNF group: 1). At 6 weeks after SCI, a rat in the injury group died during biotinylated dextran amine (BDA) tracing (3D-CC-BDNF group: 1). At 8 weeks after SCI, two rats in the injury group died during magnetic resonance imaging (MRI) (SCI group: 1, 3D-CC+BDNF group: 1). The details of the number of rats used in the experiment were shown in Supplementary Table S3. In our study, the animals were not replaced. To avoid infection, rats were injected

intraperitoneally with penicillin sodium (15 mg/kg) once a day for 7 days after surgery [39].

Behavioral assessment

The Basso–Beattie–Bresnahan (BBB) locomotion function score were conducted at 1 day before the surgery, and at 1 day, 1, 2, 3, 4, 6 and 8 weeks post-surgery and the inclined-grid climbing tests were carried out at 1 day before the surgery, and at 1 day, 1, 2, 4, 6 and 8 weeks post-surgery [40, 41] ($n = 15$ for each group). Then the bilateral hind limb movements of all rats were observed at 8 weeks after the operation. Eight weeks after surgery, five rats were randomly selected from each group. Under a microscope and under sterile conditions, the skin and muscles were cut to expose the original surgical site. Then spinal tissue that was regenerated from the surgical site was recut. The BBB tests were performed at 1, 2, 3, 4 and 5 weeks after re-cutting and the inclined-grid climbing tests were carried out at 1, 2, 3 and 4 weeks after re-cutting ($n = 5$ for each group).

Electrophysiological assays

An evoked potential meter (VIKING QUEST4, USA) was implemented to obtain motor evoked potentials (MEP) in all experimental groups ($n = 15$ for each group) 2, 4, 6, and 8 weeks after surgery. Furthermore, amplitude and latency of left and right hindlimbs were observed. The specific operation methods of electrophysiological analysis were as described above [40]. Amplitudes are very challenging to standardize between animals due to inherent conductance differences and inexact lead placements. Latency is a more reproducible measure.

MRI and diffusion tensor imaging (DTI)

Eight weeks after SCI, all MRI data were obtained by using a 3.0 T MRI scanner (MAGNETOM VERIO, SIEMENS, Germany) ($n = 15$ for each group). Data collection was carried out in areas of interest, which were damaged areas. The sequence parameters of TIWI, T2WI and DTI were based on previously reported study [31]. After scanning all the rats, the processed data was imported into a separate workstation (Advantage Windows, version 4.2; GE Healthcare, Waukesha, Wisconsin, USA) to obtain DTI data. Then the obtained data was further processed, and then processed by MATLAB, Diffusion Toolkit, and Trackvis software to obtain diffusion tensor tractography (DTT) of the spinal cord, and fractional anisotropy (FA) values and apparent diffusion coefficient (ADC) values of various segments of the spinal cord. The number of fibers traversing the section of T10 level was detected by Trackvis software. Centering on the middle of the spinal cord injury, five FA values and ADC values were measured between the rostral and caudal at 1.5 mm intervals. Finally, each rat had a total of 11 FA values and 11 ADC values. The FA map and the ADC map were obtained from the above data.

Locomotor function–imaging correlation analyses were performed according to the method previously reported [31]. Pearson correlation coefficients (R) and P values for each position were obtained to investigate possible correlations between locomotor function (BBB score of left and right hindlimbs) and imaging (FA values or ADC values).

Pathological analysis

Eight weeks post-surgery, the rats were sacrificed and transcardially perfused to obtain the spinal cord and gastrocnemius as described above [40]. The spinal cord tissue was sliced longitudinally by a cryostat microtome (Leica CM1950, Germany) to obtain sections with a thickness of 5 μm. Then, these slices were used for hematoxylin and eosin (HE) staining and Bielschowsky's silver staining for pathological examination ($n = 15$ for each group) [42]. After taking HE-stained photos, Image-Pro Plus software was used to calculate the area of the cavity of the spinal cord [43]. The SCI area (width 2 mm, length 3 mm) was chosen to calculate the cavity area. The gastrocnemius muscles of the bilateral hindlimbs were weighed. Masson trichrome staining was performed in the extracted gastrocnemius muscles ($n = 15$ for each group). For immunofluorescence staining, the 20 μm thickness tissue sections were incubated at 4°C overnight with primary antibodies anti-NF (1:200, Abcam, Cambridge, UK) (neurofilaments (axons/dendrites) marker), anti-GFAP (1:200, Abcam, Cambridge, UK) (astrocytes marker), anti-GAP43 (1:200, Abcam, Cambridge, UK)) (axon regeneration marker), anti-PSD95 (1:500, Abcam, Cambridge, UK) (postsynaptic marker postsynaptic density protein 95), anti-SYP (1:200, Abcam, Cambridge, UK) (presynaptic marker synaptophysin) and anti-MBP (1:500, Abcam, Cambridge, UK) (a very important protein on the myelin sheath, which is the necessary structure for nerve impulses to conduct along axons) ($n = 15$ for each group). For quantitative analysis, two areas (0.40 mm × 0.40 mm) were chosen at the rostral or the injury/graft site or the caudal of the SCI area at 400× magnification for each section of spinal cord (10 sections for each rat, 5 rats for each group), respectively. Image-Pro Plus was implemented to convert positive fluorescence staining areas of NF, GFAP, GAP43, PSD95, SYP and MBP into areas of interest (AOI), and measured the pixel area for each AOI. The ratio of the total pixels of the AOI to the total pixels of the area was conducted to calculate the relative density of NF, GFAP, GAP43, PSD95 and SYP positive fluorescence staining.

BDA tracing

After anesthesia, the rats in Sham group, SCI group, 3D-CC+BDNF group and 3D-CC-BDNF group were fixed on a stereotaxic frame at 6 weeks post-surgery. A total of 12 holes were drilled on the rat skull using a micro drill. 10% BDA (Cell Signaling Technology, Beverly, MA, USA) was slowly injected into 12 sites by micro-syringe (Hamilton, Switzerland). The Bregma was used as the zero point. The coordinates of these 12 points were: 2.5 mm/0.5 mm, 2.5 mm/1.5 mm, 2.5 mm/−1 mm, 3.5 mm/0. 5 mm, 3.5 mm/1.5 mm, 3.5 mm/−1 mm, −2.5 mm/0.5 mm, −2.5 mm/1.5 mm, −2.5 mm/−1 mm, −3.5 mm/0.5 mm, −3.5 mm/1.5 mm, −3.5 mm/−1 mm) (Fig. 8B). And the injection depths were 1 mm, 1.5 mm and 2.0 mm, respectively. Furthermore, the injection dose was 0.3 μl for each deep injection. Two weeks after the injection of BDA, the spinal cord was removed transcardially perfusing and fixed with 4% paraformaldehyde ($n = 5$ for each group). The spinal cord tissue was sliced longitudinally by a cryostat microtome to obtain sections with a thickness of 20 μm. To analyze the results of biotinylated dextran amine tracing, a fluorescent microscope (DMI400B, Leica, Germany) was performed to observe the sections. For quantitative analysis, the percentage of BDA positive fibers at −1 mm, −0.5 mm, 0 mm, 0.5 mm and 1 mm distance caudal to the lesion center were measured by Image-Pro Plus software. The percentage of BDA positive fibers was equal to the proportion of BDA positive staining area to the total spinal cord injury area. Five rats were used for statistical analysis and five consecutive sections of each rat were used for metrology.

Transmission electron microscopy (TEM)

Eight weeks after SCI, the tissue from the injury site was cut into small pieces ($n = 5$ for each group). Ultrathin sections were examined to observe remyelination of at the injury/graft site under a Philips CM10 electron microscope (Eindhoven, Holland) according to an established method [44]. Under ×1500 magnification, at least 10 random fields of view per sample were selected to quantify the number of myelinated axons. To analyze the number of myelinated axon, at least 10 random fields were chosen for each sample at ×1500 magnification. Image-Pro Plus software (Media Cybernetics) was used to assess myelinated axon diameter and thickness of myelin sheath.

Statistical analysis

Data were reported as mean ± standard deviation (SD) values. SPSS 15.0 was implemented for statistical analysis. *T* test or Wilcoxon were used to evaluate the significance between any two groups. One-way ANOVA analysis was conducted, followed by Bonferroni analysis to perform multi-group comparisons. The *p* values of less than 0.05 were regarded as significant statistical difference.

Results

3D-CC-BDNF exhibited favorable physical properties and suitable biodegradability

3D-CC-BDNF was manufactured by a 3D printer (Fig. 1A–C). Then 3D-CC-BDNF needed to be freeze-dried to form (Fig. 1D). The images of light microscopy (Fig. 1E), fluorescent microscope (Fig. 1F–G), SEM (Fig. 1H–M) and HE staining (Fig. 1N–O) revealed 3D-CC-BDNF was porous, which provided a good environment for cell growth and adhesion.

The biodegradability of the five mass ratios of scaffolds was determined by changes in scaffold mass over 8 weeks (Supplementary Fig. S2). Different degradation among the scaffolds with five mass ratios was observed. Eight weeks after transplantation, 3D-CC-BDNF scaffolds with three of five mass ratios (collagen: chitosan = 1:5, 1:2, 1:1) had not been completely degraded. Four weeks after implantation, 3D-CC-BDNF scaffolds with the mass ratio of collagen:chitosan = 5:1 was completely degraded. Six weeks after implantation, 3D-CC-BDNF scaffolds with the mass ratio of collagen:chitosan = 2:1 was completely degraded. These results indicated that the degradation rate of 3D-CC-BDNF increased with the mass ratio of collagen to chitosan. The degradation time of 3D-CC-BDNF scaffolds with the mass ratio of collagen:chitosan = 2:1 was suitable for SCI repair process. Therefore, 3D-CC-BDNF scaffolds with the mass ratios (collagen:chitosan = 2:1) were chosen as the scaffolds for subsequent experiments.

The water absorption of 3D-CC-BDNF was lower than that of 3D-C-BDNF and 3D-C + BDNF ($P < 0.05$), which was conducive to maintaining BDNF (Fig. 1P). The porosity of the 3D-CC-BDNF was higher than that of 3D-C-BDNF and 3D-C+BDNF ($P < 0.05$), which facilitated the diffusion of nutrient solution and the formation of tissue (Fig. 1Q) [45]. There is no significant difference between 3D-CC-BDNF and 3D-CC+BDNF in water absorption and porosity (Fig. 1P and Q). To evaluate the mechanical properties of the scaffolds, the compressive strain–compressive stress curve and elastic modulus of the scaffolds were obtained by an Instron 5865 mechanical tester (Fig. 1R). Compared with C + BDNF ((16.58 ± 4.70) kPa), CC + BDNF ((28.91 ± 5.31) kPa) and 3D-C-BDNF ((53.56 ± 6.01) kPa), the elastic modulus of 3D-CC-BDNF ((64.16 ± 5.27) kPa ($P < 0.05$)) was enhanced (Fig. 1S), which provided a good internal environment for the repair of tissue damage. The apex of the endothermic change caused by temperature was expressed as Tm, and the peak was due to the denaturation of the BDNF. Tm was widely used as a marker for the stability of proteins against denaturation caused by temperature changes. The Tm value of pure BDNF (Fig. 1T) was 5°C lower than that of 3D-CC-BDNF, suggesting that integrated 3D printed collagen/chitosan BDNF scaffold increased the stability of BDNF. In the infrared spectrum of 3D-CC+BDNF and 3D-CC-BDNF (Fig. 1U), the absorption peak of 1500–850 cm^{-1} might be a stretching vibration of C = O, but C = C double bond, water peak, and amino peak might also appear here. The peak of 1300–1500 cm^{-1} was related to the C–H stretching. The absorption peak of 1000–1300 cm^{-1} was the presence of C–O. The peaks at around 3413.229 cm^{-1} and 3441.587 cm^{-1} were attributed to the stretching of the C-OH. The absorption peak at 3441.587 cm^{-1} in the FTIR-ATR spectrum of 3D-CC-BDNF (Fig. 1U) was markedly higher than that of 3D-CC+BDNF, which indicated that more hydrogen bonds in 3D-CC-BDNF might be formed between collagen/chitosan and BDNF compared to 3D-CC+BDNF.

Low temperature 3D printing could improve the ability of collagen/chitosan to fix and absorb BDNF

In the 3D-CC-BDNF group, higher release (5.575% of BDNF) (Fig. 1V) was observed at the first day, and a high and stable release was observed for a long time (Fig. 1W). The release of 3D-CC+BDNF was relatively low (0.82% of BDNF) at the first day (Fig. 1V). Although the 3D-CC+BDNF group could also release a certain amount of BDNF, it was not guaranteed to have a stable and sufficient amount of BDNF release (Fig. 1W).

3D-CC-BDNF could markedly increase the BDNF concentration in spinal cord tissue *in vivo*

The *in vivo* release of BDNF from 3D-CC-BDNF and 3D-CC+BDNF was compared in SCI model. The BDNF concentration (ng/mg spinal cord tissue) for spinal cord tissue was measured at five different time points (Fig. 1X). The implantation of 3D-CC-BDNF prominently increased the BDNF concentration in spinal cord tissue compared to the implantation of 3D-CC+BDNF ($P < 0.01$). The *in vivo* release results suggested that 3D-CC-BDNF could effectively ameliorate the bioavailability of BDNF.

3D-CC-BDNF exhibited good cytocompatibility *in vitro*

Immunofluorescence experiments suggested that the cultured neurospheres were Nestin-positive (Fig. 2A). Under the phase contrast microscope, HUCMSCs were fusiform, and the cells were closely connected to form a spiral arrangement (Supplementary Fig. S4A). Flow cytometry showed that HUCMSCs are positive for CD90, CD105 and CD73, fulfilling the criteria for mesenchymal stem cells (Supplementary Fig. S3B). The expression of CD90 and CD105 on HUCMSCs were also confirmed by immunofluorescence staining (Supplementary Fig. S4C–D). Seven days after co-culture, the phase contrast microscope, SEM, HE staining and immunofluorescence staining showed that NSCs and HUCMSCs grow on the surface and the inside of the pore of the scaffolds (Fig. 2B–E, Supplementary Fig. S4E–L), which indicated that the NSCs or HUCMSCs grew well on the scaffolds with good cell morphology. Compared to 3D-CC+BDNF, the number of NSCs and HUCMSCs adhering to 3D-CC-BDNF was significantly increased (Fig. 2B–E, Supplementary Fig. S4E–L). As the co-culture time prolonged, cell adhesion rate of

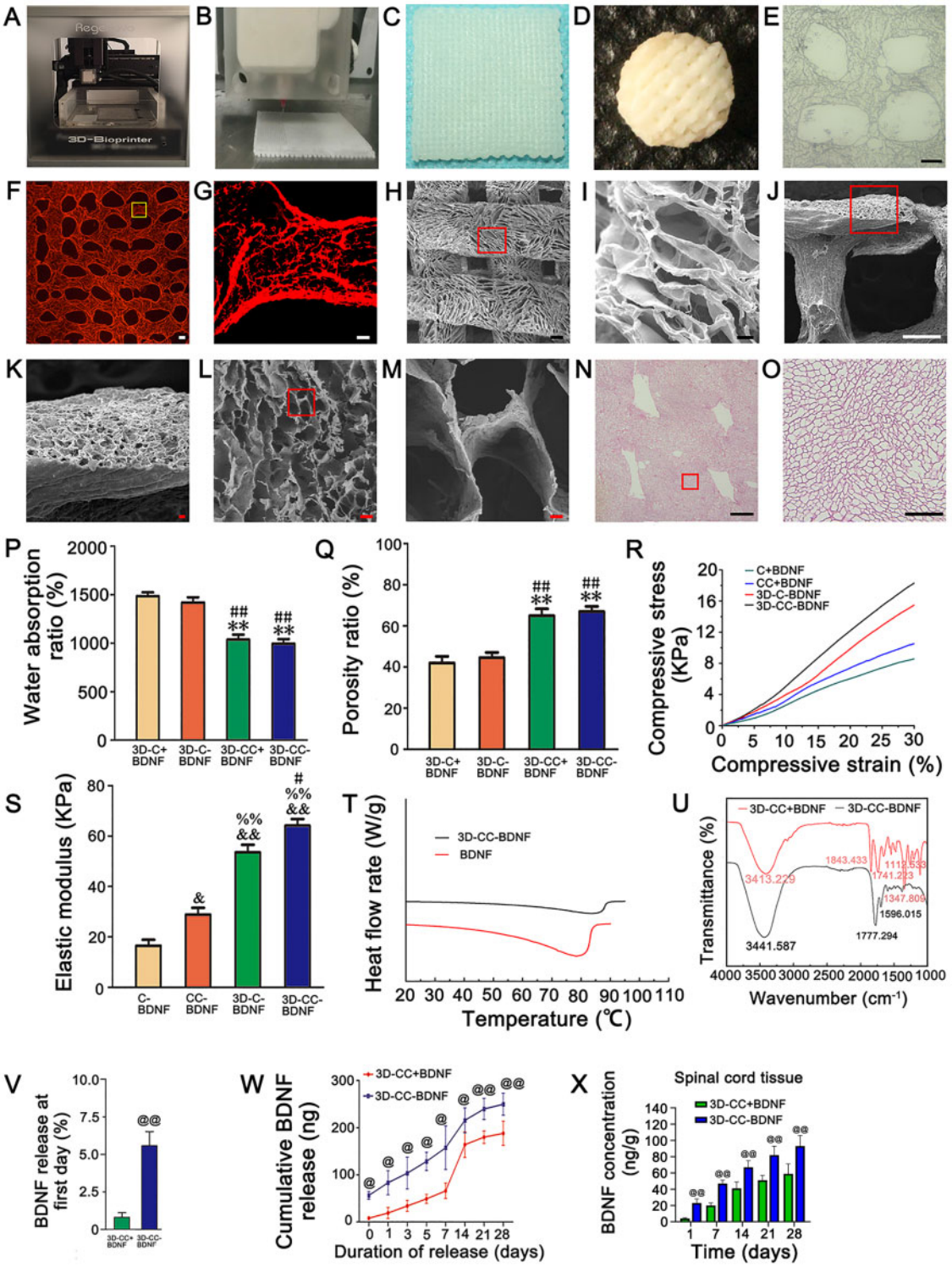

Figure 1. The properties of scaffolds. (**A**) 3D printer for scaffold preparation. (**B, C**) 3D-CC-BDNF fabricated by a 3D printer. (**D**) 3D-CC-BDNF was freeze dried by a freeze dryer. (**E–J**) The images of light microscopy (E), fluorescent microscope (F–G), SEM (**H–M**) and HE staining (**N–O**) revealed were porous microstructure of 3D-CC-BDNF. G was an amplified image of the yellow box in F. (I, K, M, O) were an amplified image of the red box in (H, J, L, N), respectively. (**P–S**) The water absorption (P), the porosity (Q), the compressive strain–compressive stress curve (R), and the elastic modulus (S) of the scaffolds. (**T**) Differential scanning calorimetry curve of BDNF and 3D-CC-BDNF during heating. (**U**) Infrared spectra of 3D-CC-BDNF and 3D-CC+BDNF. (**V**) Percentage of BDNF released from 3D-CC-BDNF and 3D-CC+BDNF at first day. (**W**) Total amount of cumulative release of BDNF within 28 days. (**X**) BDNF concentration-time curve for spinal cord tissue after injection. Data were presented as mean ± SD; $n=3$. $^{**}P<0.01$ vs 3D-C+BDNF. $^{\#}P<0.05$, $^{\#\#}P<0.01$ vs 3D-C-BDNF. $^{\&}P<0.05$, $^{\&\&}P<0.01$ vs C-BDNF. $^{\%\%}P<0.01$ vs CC-BDNF. $^{@}P<0.05$, $^{@@}P<0.01$ vs 3D-CC+BDNF. Scale bars = 300 μm in panels (E, F, H, J, N), 50 μm in panels (G, I, K, L, O), 5 μm in panel M. n = number of animals under each condition (n is expressed as dots in the bars) in X, $n=10$.

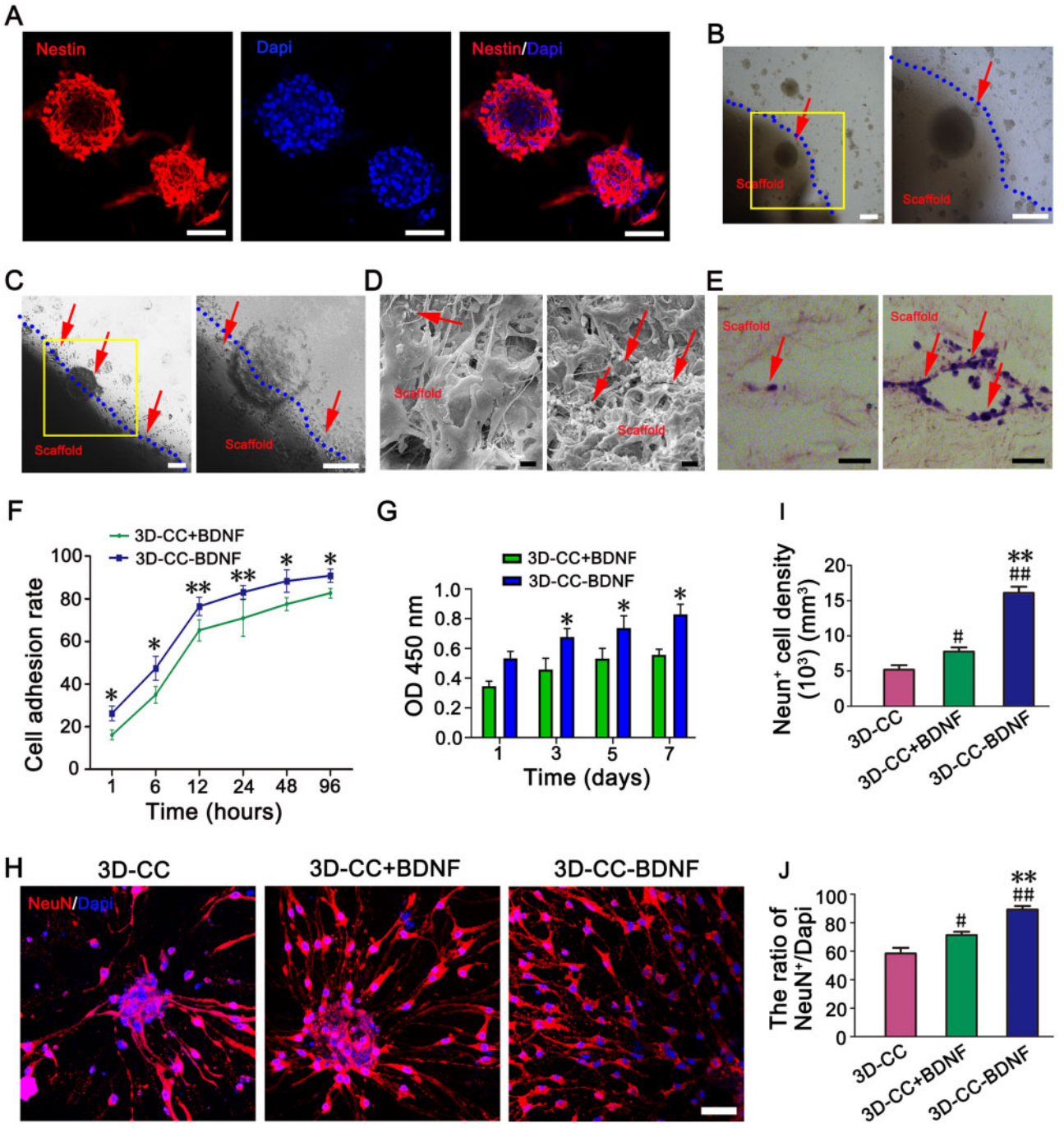

Figure 2. Biocompatibility test of scaffolds and neural stem cells *in vitro*. (**A**) Identification of NSCs, immunographs of neurospheres stained with nestin antibody (red) and nucleus stained with dapi antibody (blue). (**B, C**) morphological observation of NSCs cultured on 3D-CC+BDNF (B) and 3D-CC-BDNF (C) under a phase contrast microscope. The image on the right was an amplified image of the yellow box in the image on the left. (**D**) Scanning electron microscopy observation of NSCs growth status in 3D-CC+BDNF (left) and 3D-CC-BDNF (right). (**E**) HE staining observation of 3D-CC+BDNF (left) and 3D-CC-BDNF (right) co-cultured with NSCs. All red arrows showed NSCs. (**F**) Cell adhesion rates of NSCs after incubation with 3D-CC+BDNF (left) and 3D-CC-BDNF (right) at 1, 6, 12, 24, 48 and 96 h after co-culture. (**G**) Light absorbance of NSCs in 3D-CC+BDNF and 3D-CC-BDNF co-cultured with NSCs at 1, 3, 5 and 7 days after co-culture. (**H–J**) The image of NeuN (red) immunofluorescence staining. Mature neurons were identified by immunostaining with anti-NeuN antibody (red) (H) at 2 weeks after co-culture. Dapi antibody (blue) was performed to counter-stain cell nuclei (H) at 2 weeks after co-culture. Quantification of the $NeuN^+$ cell density (I) and the ratio of $NeuN^+$/dapi (J). Data were presented as mean ± SD, $n = 5$. $^{*}P < 0.05$, $^{**}P < 0.01$ vs 3D-CC+BDNF. $^{\#}P < 0.05$, $^{\#\#}P < 0.01$ vs 3D-CC. Scale bars = 50 μm in panels (A, B, C, E, H), 5 μm in panel (D).

NSCs in 3D-CC+BDNF and 3D-CC-BDNF was increased. Compared to 3D-CC+BDNF, cell adhesion rate of NSCs in 3D-CC-BDNF was prominently more at the same time ($P < 0.05$) (Fig. 2F). As the co-culture time prolonged, the higher light absorbance of NSCs or HUCMSCs in the two groups was observed (Fig. 2G, Supplementary Fig. S4M). The light absorbance of NSCs or

HUCMSCs in the 3D-CC-BDNF group was enhanced compared to the 3D-CC+BDNF group ($P < 0.05$) 3, 5 and 7 days after the co-culture. The results of CCK-8 showed that both scaffolds had cytocompatibility and 3D-CC-BDNF group was more conducive to cell growth compared to 3D-CC+BDNF group. These results indicated that NSCs or HUCMSCs grew well on both scaffolds, and neither of the scaffolds had significant cytotoxicity.

3D-CC-BDNF up-regulated immature and mature neuronal markers *in vitro*

To elucidate the underlying mechanism by which 3D-CC-BDNF could release more BDNF to promote the survival and maturation of NSCs compared with 3D-CC+BDNF and 3D-CC, 3D-CC, 3D-CC+BDNF or 3D-CC-BDNF were co-cultured with the same amount of purified NSCs *in vitro*, respectively. Anti-DCX antibodies and Anti-NeuN antibodies were immunostained to detect immature and mature neurons, respectively. Compared with 3D-CC+BDNF and 3D-CC, both DCX^+ cell density and the ratio of DCX^+/Dapi in 3D-CC-BDNF showed a significant increase at 7 days after co-culture (Supplementary Fig. S3A–C). The $NeuN^+$ cell density and the ratio of $NeuN^+$/Dapi in 3D-CC-BDNF were also markedly increased compared with 3D-CC+BDNF and 3D-CC at 2 weeks after co-culture (Fig. 2H–J). The results demonstrated that 3D-CC-BDNF could efficiently induce NSCs to differentiate immature and mature neurons.

3D-CC-BDNF transplantation ameliorated locomotor function after SCI

One day after SCI, the bilateral hind limbs of all SCI rats were paralyzed, while the bilateral hind limbs of Sham group were normal. Both behavioral assessment and electrophysiological studies demonstrated that the 3D-CC-BDNF group showed better locomotor function recovery compared with the 3D-CC+BDNF group (Figs 3A–G and 4A–E). Compared to implanting 3D-CC+BDNF or without implanting scaffolds, implanting 3D-CC-BDNF could significantly increase the BBB scores of right and left hindlimbs from 2 to 8 weeks after surgery (Fig. 3A–B). Eight weeks post-surgery, the 3D-CC-BDNF group for right hindlimbs exhibited the best motor functional recovery, with significantly higher BBB scores than the SCI group ($P < 0.01$) and the 3D-CC+BDNF group ($P < 0.01$) (Fig. 3C–D). To demonstrate that elevated BBB scores were associated with regenerated nerve fibers rather than the compensatory effect below the lesion area or promoting functional recovery by BDNF modulate spinal cord neurons below lesion, retransection was carried out at 8 weeks after SCI. Regenerated nerve bundles were retransected. The BBB score of SCI group, the 3D-CC+BDNF group and the 3D-CC-BDNF group felled to the complete SCI level at the first day after re-cutting, and kept this low level for the next five weeks (Fig. 3A–B). The results of re-cutting proved that the recovery of locomotor function was related to the regenerated nerve fibers rather than the compensatory effect below the lesion area or promoting functional recovery by BDNF modulate spinal cord neurons below lesion [46].

For the inclined-grid climbing test, compared with implantation of 3D-CC+BDNF or without implantation, the implantation of 3D-CC-BDNF could further prominently increase the angle of the slope (Fig. 3E). Eight weeks post-surgery, the 3D-CC-BDNF group exhibited the best motor functional recovery, with significantly higher slope angle than the SCI group ($P < 0.01$) and the 3D-CC+BDNF group ($P < 0.01$) (Fig. 3F). Similar to the BBB score, the slope angle of SCI group, 3D-CC+BDNF group and 3D-CC-BDNF group felled to the complete SCI level on the first day after re-cutting, and kept this low level for the next four weeks (Fig. 3E).

The hindlimbs of 3D-CC-BDNF group and 3D-CC+BDNF group exhibited the ability to walk autonomously, while the hindlimbs of the SCI group did not demonstrate the ability to walk autonomously (Fig. 3G) [47]. These results indicated that the implantation of 3D-CC-BDNF could significantly improve locomotor function after complete spinal cord transection.

The amplitude and latency of MEP are usually assessed to reflect the number of excited axons and the nerve conduction velocity, respectively. Eight weeks after SCI, compared with the SCI group (amplitude: 0.09 ± 0.02 mV; latency: 18.33 ± 0.63 ms), the amplitude and latency of left hindlimb in the 3D-CC+BDNF group (amplitude: 0.15 ± 0.02 mV, $P < 0.01$; latency: 15.67 ± 0.85 ms, $P < 0.05$) and 3D-CC-BDNF group (amplitude: 0.20 ± 0.02 mV, $P < 0.01$; latency: 12.12 ± 1.15 ms, $P < 0.01$) (Fig. 4A, B, D) showed a significant improvement. Eight weeks after SCI, implanting 3D-CC-BDNF scaffolds could markedly augment the amplitude and shorten the latency (amplitude: $P < 0.01$; latency: $P < 0.01$) compared with implanting 3D-CC+BDNF (Fig. 4A, B, D). Eight weeks after surgery, the statistical differences in amplitude and latency of the right hind limb between the three groups were similar to those of the left hind limb. Statistical differences in the amplitude and the latency at 2, 4 and 6 weeks after SCI were similar to those at 8 weeks after SCI (Fig. 4A–E). These data suggested that the implantation of 3D-CC-BDNF scaffolds improved locomotor function after complete spinal cord transection.

Transplantation of 3D-CC-BDNF promoted regeneration of nerve fibers tracts after SCI

Macroscopic MRI

It was observed in both T1WI and T2WI that the 3D-CC-BDNF group and the 3D-CC+BDNF group markedly had more connections than the SCI group, and the density of connection in the 3D-CC-BDNF group was slightly higher than that of the 3D-CC+BDNF group at 8 weeks after SCI. The SCI group demonstrated little connection from the rostral to the caudal at the injury site. The 3D-CC-BDNF group showed significant continuity at the injury site. (Fig. 5A and B). Compared to the SCI group and the 3D-CC+BDNF group, 3D-CC-BDNF group was more continuous and the signal strength of 3D-CC-BDNF group was closer to the Sham group (Fig. 5A and B).

Microscopic DTI

For the DTT, compared to the SCI group (17.33 ± 6.807) and the 3D-CC+BDNF group (37.66 ± 4.933), the 3D-CC-BDNF group (87.33 ± 11.015, $P < 0.01$) markedly had more regenerative nerve fiber tract passing from the rostral of the spinal cord to the caudal of the spinal cord at 8 weeks after SCI (Fig. 5E). Furthermore, in terms of the number and continuity of nerve fiber tracts, the 3D-CC-BDNF group was closest to the Sham group (Fig. 5C–E). At these locations (6 mm, 1.5 mm, −3 mm, −4.5 mm and −7.5 mm from the epicenter of the injury site), the implantation of 3D-CC-BDNF group prominently increased the FA values compared to the implantation of 3D-CC+BDNF and without any scaffolds implantation ($P < 0.05$) (Fig. 5F). The ADC value of 3D-CC-BDNF group was markedly smaller than that of the SCI group and 3D-CC+BDNF

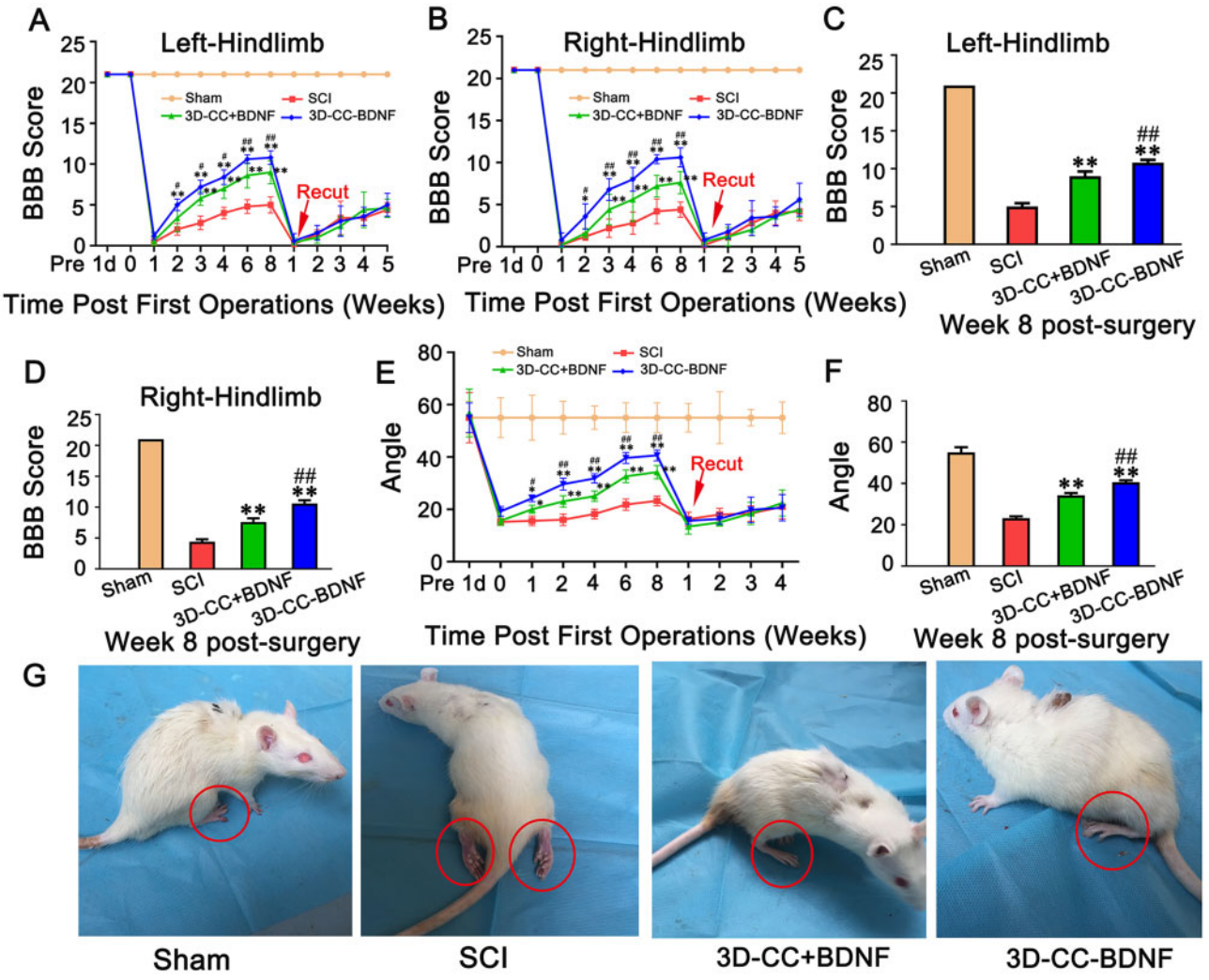

Figure 3. Behavioral assessment in the sham group, SCI group, 3D-CC+BDNF group and 3D-CC-BDNF group after the operation. (**A, B**) BBB open-field walking scores of left hindlimbs (A) and right hindlimbs (B) at 1 day before the operation, and at 1 day, 1, 2, 3, 4, 6 and 8 weeks after the operation, and at 1, 2, 3, 4 and 5 weeks after re-cutting. (**C, D**) BBB open-field walking scores of left hindlimbs (C) and right hindlimbs (D) at 8 weeks after the operation. (**E**) The inclined-grid climbing test at 1 day before the operation, and at 1 day, 1, 2, 4, 6 and 8 weeks after the operation, and at 1, 2, 3 and 4 weeks after re-cutting. (**F**) The inclined-grid climbing test at 8 weeks after the operation. (**G**) Typical picture of rats in the four groups at 8 week after the operation. $^{*}P < 0.05$, $^{**}P < 0.01$ vs SCI group. $^{\#}P < 0.05$, $^{\#\#}P < 0.01$ vs 3D-CC+BDNF group. n = number of animals under each condition (n is expressed as dots in the bars); in A–F, $n = 15$.

group ($P < 0.05$) at these locations (−3 mm, −4.5 mm, −6 mm and −7.5 mm from the epicenter of the injury site) (Fig. 5G). The results of FA and ADC values were consistent with those of MRI and DTT images.

To explore the possible correlations between locomotor function (BBB score of left and right hindlimbs) and imaging (FA values or ADC values), corresponding Pearson correlations (R) of all positions was plotted (Fig. 5H–K), followed by calculating the average of Pearson correlation coefficient (R). The results of Pearson correlation coefficient (R) obtained were as follows: (mean ± SD), BBB (left hindlimb) versus FA: 0.96 ± 0.02, BBB (right hindlimb) versus FA: 0.95 ± 0.02, BBB (left hindlimb) versus ADC: −0.94 ± 0.01, BBB (left hindlimb) versus ADC: −0.95 ± 0.01. *P*-values for all positions calculated for all locations indicating that each correlation was statistically significant ($P < 0.0001$). Positive correlations between locomotor function (BBB score of left and right hindlimbs) and imaging (FA values or ADC values) from the rostral to the caudal were observed after 8 weeks of SCI.

Implanting 3D-CC-BDNF could fill the gap of the injury site, facilitate nerve fiber regeneration and accelerate the establishment of synaptic connections

Eight weeks after surgery, the tissue at the injury site in the 3D-CC-BDNF group was full, smooth, and not easy to be broken, which was not observed in the SCI group and the 3D-CC+BDNF group. The tissue at the injury site in the 3D-CC-BDNF group adhered lightly to the surrounding tissue. The tail of spinal cord was concentrated and is not easily broken (Fig. 6A). Furthermore, when the tissues at the injury site in the SCI group and the 3D-CC+BDNF was taken, it adhered more tightly to the surrounding tissues and the tail of spinal cord was scattered and fragile (Fig. 6A). For HE staining, we observed that the tissue at the injury site in the 3D-CC-BDNF group was more continuous and had fewer coloboma compared with SCI group and 3D-CC+BDNF group (Fig. 7B). Compared to the SCI group (4.278 ± 0.619 mm^2) and the 3D-CC+BDNF group (2.564 ± 0.785 mm^2), the average cavity area of the 3D-CC-BDNF group (1.546 ± 0.547 $mm^{2)}$ was significantly smaller (Fig. 6C),

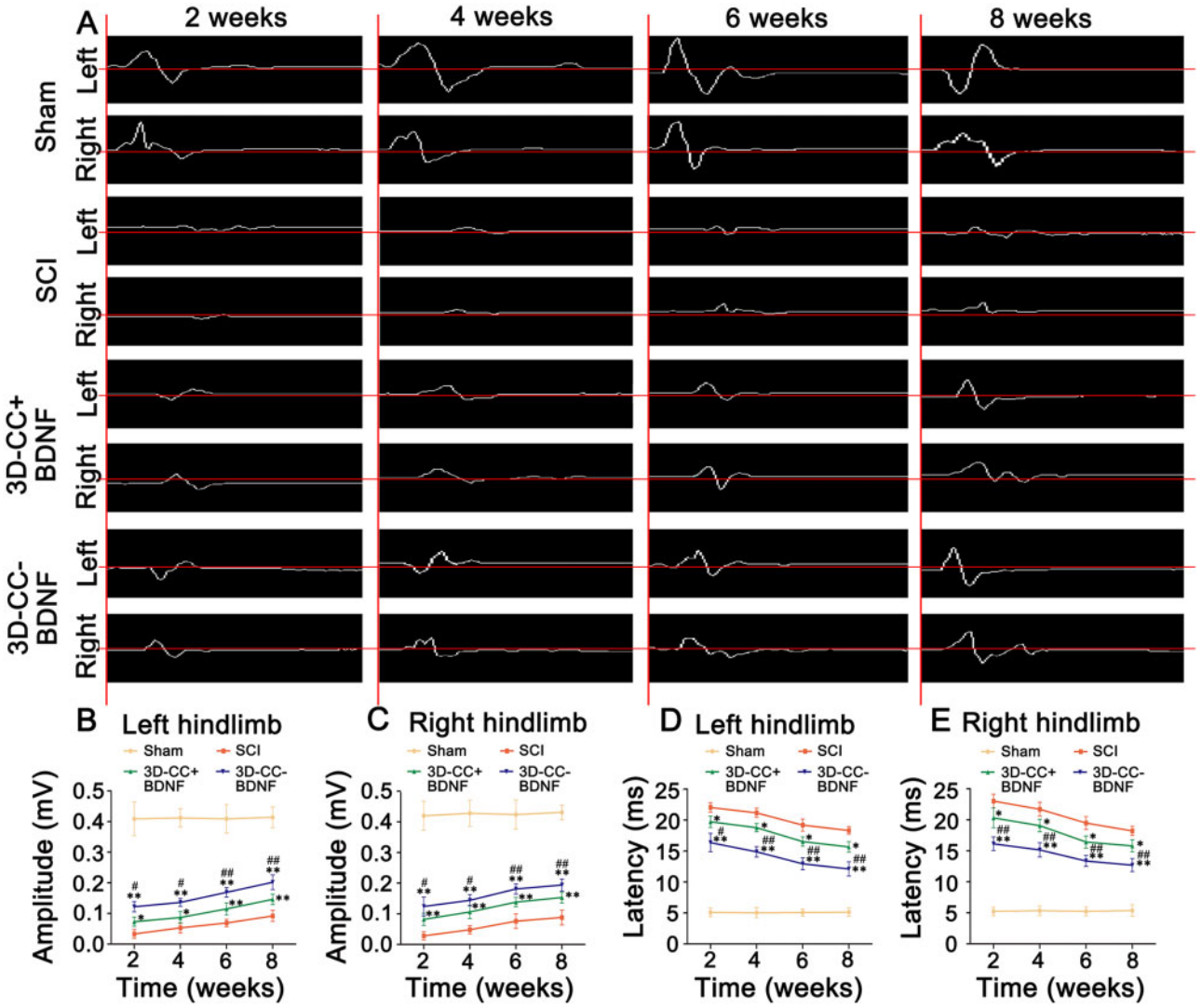

Figure 4. Electrophysiological studies at 2, 4, 6 and 8 weeks after SCI. (**A**) Representative pictures of MEP traces of left hindlimb and right hindlimb. (**B–E**) The amplitude and the latency of left hindlimb (B, D) and right hindlimb (C, E). $^{*}P < 0.05$, $^{**}P < 0.01$ vs SCI group. $^{\#}P < 0.05$, $^{\#\#}P < 0.01$ vs 3D-CC+BDNF group. n = number of animals under each condition (n is expressed as dots in the bars); in A–E, $n = 15$.

which indicated that implantation of 3D-CC-BDNF scaffolds significantly reduced cavity formation at the injury site. Bielschowsky's silver staining showed that the nerve fibers at the injury site were significantly increased in the 3D-CC-BDNF group compared to SCI group and the 3D-CC+BDNF group (Fig. 6D), which indicated implanting 3D printed collagen/chitosan scaffold integrated with BDNF could fill the cavity of the injury site and promote the regeneration of nerve fiber.

After spinal cord transection, the function of bilateral hindlimbs was lost, the muscles were disused and the weight gradually decreased (Fig. 6E). With the gradual recovery of spinal cord function, the activities of bilateral hindlimbs were gradually increased and the function of muscle was gradually improved. Comparing the weight of the gastrocnemius muscle can reflect the recovery of SCI. Compared with the SCI group and 3D-CC+BDNF group, the weight of bilateral gastrocnemius muscle in the 3D-CC-BDNF group was significantly higher ($P < 0.05$) (Fig. 6F–G). Masson's trichrome staining of the gastrocnemius muscle showed that the 3D-CC-BDNF group had increased muscle fiber density and reduced the degree of atrophy when compared with the SCI group and 3D-CC+BDNF group (Fig. 6H).

Immunofluorescence staining indicated that implanting 3D-CC-BDNF could significantly increase the number of NF-positive nerve fibers when compared with implanting 3D-CC+BDNF scaffolds and without implanting scaffolds, regardless of the rostral area, at the injury/graft site or the caudal area of spinal cord at 8 weeks post-surgery (Fig. 7A–E, A1–A3, B1–B3, C1–C3, D1–D3). Reduced amount of GFAP-positive glia scar and increased GAP43 immunoreactivity at the injury/graft site were observed in the 3D-CC-BDNF group (Fig. 7F–H). These results indicated that implanting 3D-CC-BDNF could create a good microenvironment to promote nerve fiber regeneration and reduce glial scar formation.

To investigate whether 3D-CC-BDNF facilitated synaptic connections at the injury site, expression of PSD95 and SYP in the rostral area, the injury/graft site, and caudal area of spinal cord were evaluated by immunofluorescence. The expression of both PSD95 and SYP were up-regulated in the 3D-CC-BDNF group compared to the 3D-CC+BDNF group, suggesting the implantation of 3D-CC-BDNF

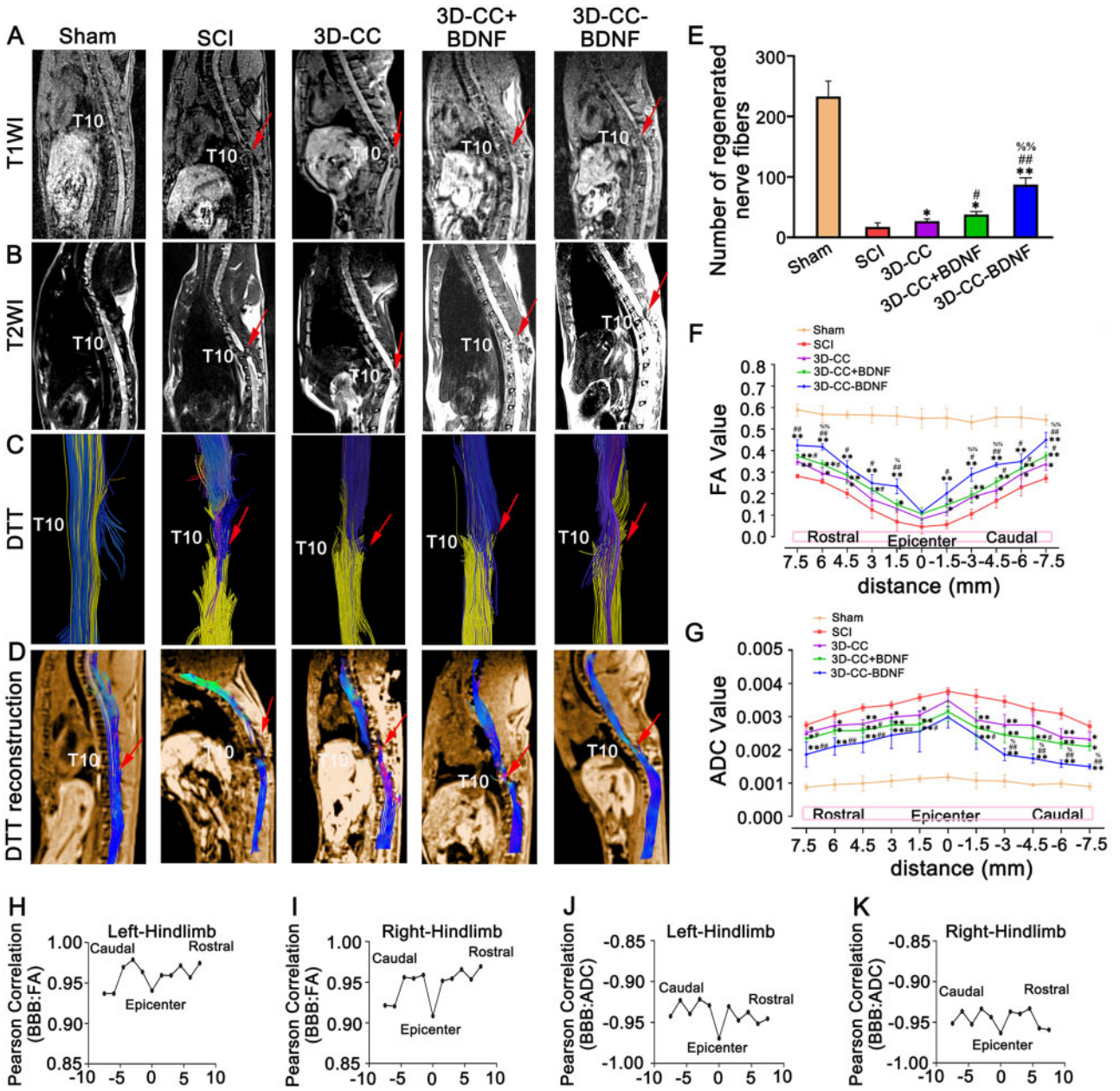

Figure 5. Magnetic resonance imaging (MRI) and diffusion tensor imaging (DTI) at 8 weeks after SCI. (**A–D**) Representative T1-weighted images (A), T2-weighted images (B), diffusion tensor tractgraphy (DTT) images (C) and DTT reconstruction images (D). (**E**) The number of regenerated nerve fibers at the injury site. (**F–G**) FA value distribution map (F) and ADC value distribution map (G) of the corresponding location at the injury site. (**H–K**) Corresponding Pearson correlation coefficient values (R) at all locations for (BBB versus FA and BBB versus ADC) of left hindlimb (H, J) and right hindlimb (I, K) were plotted. All red arrows indicated the injury/graft site located at T10 spinal cord segment. $^{*}P<0.05$, $^{**}P<0.01$ vs SCI group. $^{\#}P<0.05$, $^{\#\#}P<0.01$ vs 3D-CC group. $^{\%}P<0.05$, $^{\%\%}P<0.01$ vs 3D-CC+BDNF group. $n=$ number of animals under each condition (n is expressed as dots in the bars); in A–K, $n=15$.

promoted the maintenance and establishment of synaptic connections at the injury site (Fig. 8A–F).

In order to observe the structure of nerve fibers wrapped by myelin sheath structure, double-labeled immunofluorescence staining of NF and MBP in the rostral area, the injury/graft site and caudal area of spinal cord were performed. Furthermore, the number of NF-positive nerve fibers wrapped by MBP positive myelin sheath structures in Sham group, SCI group, 3D-CC+BDNF group, and 3D-CC-BDNF group were counted. At the injury/graft site, more NF-positive nerve fibers wrapped by MBP positive myelin sheath structures were observed in the 3D-CC-BDNF group than that in the SCI group and the 3D-CC+BDNF group (Fig. 9A–D, A1–A3, B1–B3, C1–C3, D1–D3). These results indicated that implantation of 3D-CC-BDNF could provide a suitable microenvironment favoring the regeneration of nerve fibers and myelin sheath at the injury/graft site.

Twelve positions of the BDA injection and the position of Bregma were shown in Fig. 9E. Corticospinal tracts (CST) located in

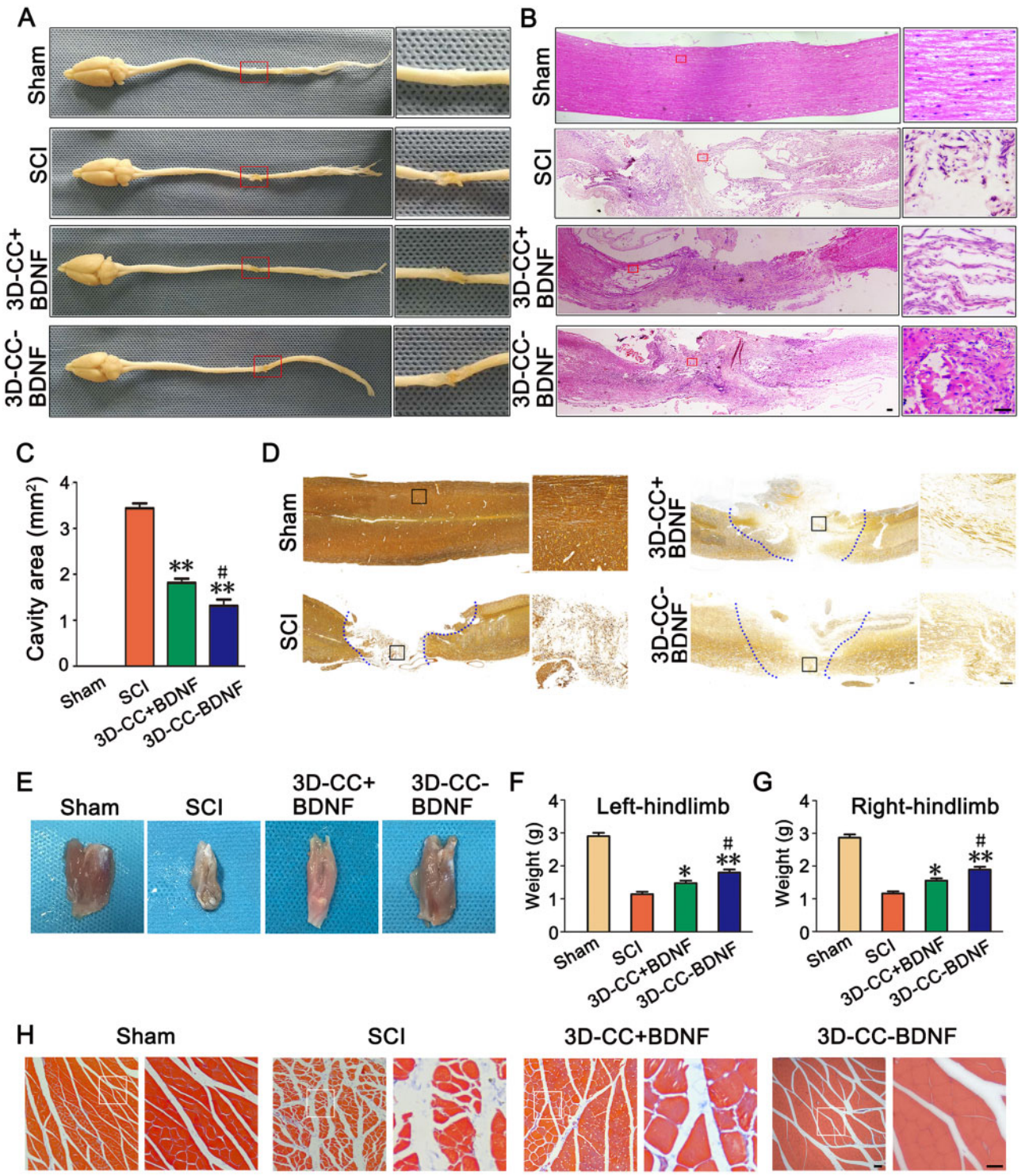

Figure 6. Histological analysis for four groups. (**A**) Macroscopic histology images of spinal cord. Low magnification of spinal cord sections (left) and higher magnification of the red boxed sections (right). (**B**) Typical HE staining images. Low magnification (50×) of spinal cord sections (left) and higher magnification (400×) of the red boxed sections (right). (**C**) Cavity area of spinal cord injury area in HE staining image. (**D**) Representative Bielschowsky's silver staining images. The image on the right was an amplified image of the black box in the image on the left. (E) Macroscopic histology images of the gastrocnemius muscle. (**F–G**) The weight of the gastrocnemius muscle of left hindlimb (F) and right hindlimb (G). (**H**) Representative Masson's trichrome staining images of the gastrocnemius muscle. Low magnification (100×) of gastrocnemius muscle sections (left) and higher magnification (200×) of the white boxed sections (right). $^{*}P < 0.05$, $^{**}P < 0.01$ vs SCI group. $^{\#}P < 0.05$ vs 3D-CC+BDNF group. Scale bars = 50 μm in panels (B, D, H). n = number of animals under each condition (n is expressed as dots in the bars); in A–H, $n = 15$.

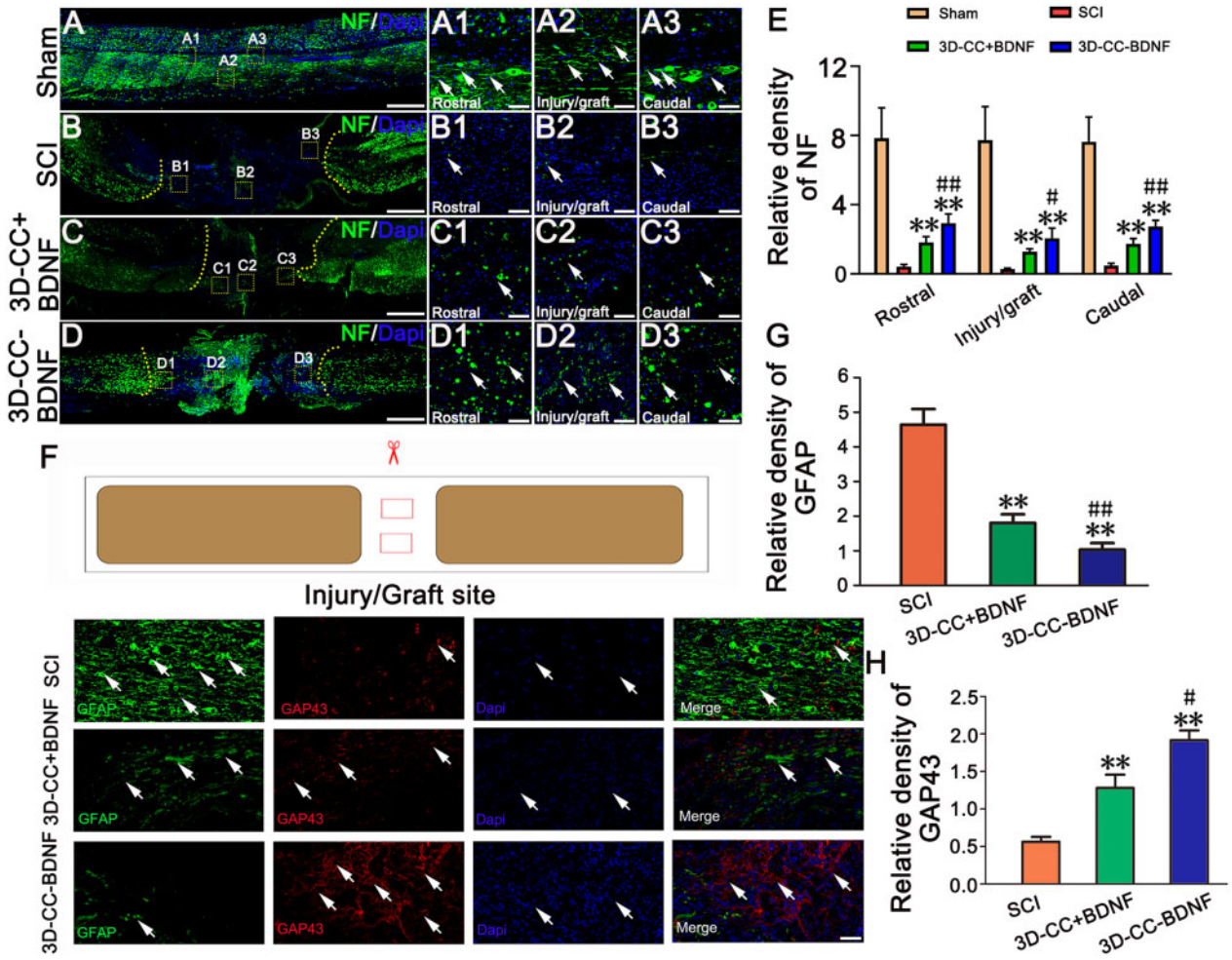

Figure 7. Immunofluorescence staining of spinal cord injury area at 8 weeks post-surgery. (**A–D**, A1–A3, B1–B3, C1–C3, D1–D3) The representative images of NF-positive nerve fibers (green, white arrow) immunofluorescence staining in longitudinal sections of spinal cord. (A1–A3), (B1–B3), (C1–C3) and (D1–D3) were an amplified image of the yellow box in (A–D), respectively, demonstrating the NF-positive staining in the rostral area, the injury/graft site and caudal area of spinal cord. (**E**) The quantification of the relative density of NF-positive nerve fibers in the rostral area, the injury/graft site and caudal area of spinal cord. (**F**) Representative images of GFAP (green, white arrow) and GAP43 (red, white arrow) immunofluorescence staining at the injury/graft site of spinal cord. (**G–H**) The quantification of the relative density of GFAP (G) and GAP43 (H) in the injury/graft site of spinal cord. $^{**}P < 0.01$ vs SCI group. $^{\#}P < 0.05$, $^{\#\#}P < 0.01$ vs 3D-CC+BDNF group. Scale bars = 500 μm in panels (A–D), 50 μm in panels (A1–A3, B1–B3, C1–C3, D1–D3, F). n = number of animals under each condition (n is expressed as dots in the bars); in A–H, $n = 15$.

the right funiculus of white matter of spinal cord could be positively stained with BDA. BDA positive CST fibers in the spinal cord injury area could be considered as markers of axonal plasticity. For evaluating the CST regeneration, the BDA tracing was performed at 6 weeks post-surgery. In the SCI group, BDA positive CST fibers were sparse in the spinal cord injury area. Conversely, implanting 3D-CC+BDNF and 3D-CC-BDNF, and especially implanting 3D-CC-BDNF demonstrated many BDA positive CST fibers in the spinal cord injury area (Fig. 9F). The BDA positive CST fibers of the 3D-CC-BDNF group (21.8 ± 2.490%) at 1 mm distance caudal to the lesion center were significantly more than that of the SCI group (6 ± 1.732%) and the 3D-CC+BDNF group (13.4 ± 2.702%) (Fig. 9F and G).

Transplantation of 3D-CC-BDNF enhanced remyelination at the injury site

It is well known that remyelination of regenerative axons is an important cause of physiological function recovery. TEM analysis demonstrated that more myelinated axons, bigger diameter of myelinated axons and thicker myelin sheath were observed at the injury site in 3D-CC-BDNF group (Fig. 9H–K). 3D-CC-BDNF group had many unmyelinated nerve fibers that tended to appear around the myelinated nerve fibers. Neuron-like cells with associated synapse-like structures were observed only in the 3D-CC-BDNF group (Fig. 9H). These results suggested that implanting 3D-CC-BDNF could promote nerve fiber regeneration, axonal ingrowth and myelination of new axons at the injury site.

Discussion

SCI often leads to motor dysfunction and other disabilities. Growth factors-loaded scaffolds were widely developed to promote SCI repair [7, 41]. The quantity of absorbed growth factors released by 3D printed scaffolds is lower than the requirement of biological effects, and the releasing process is unstable. Therefore, we try to explore whether 3D printed scaffolds integrated with growth factors can

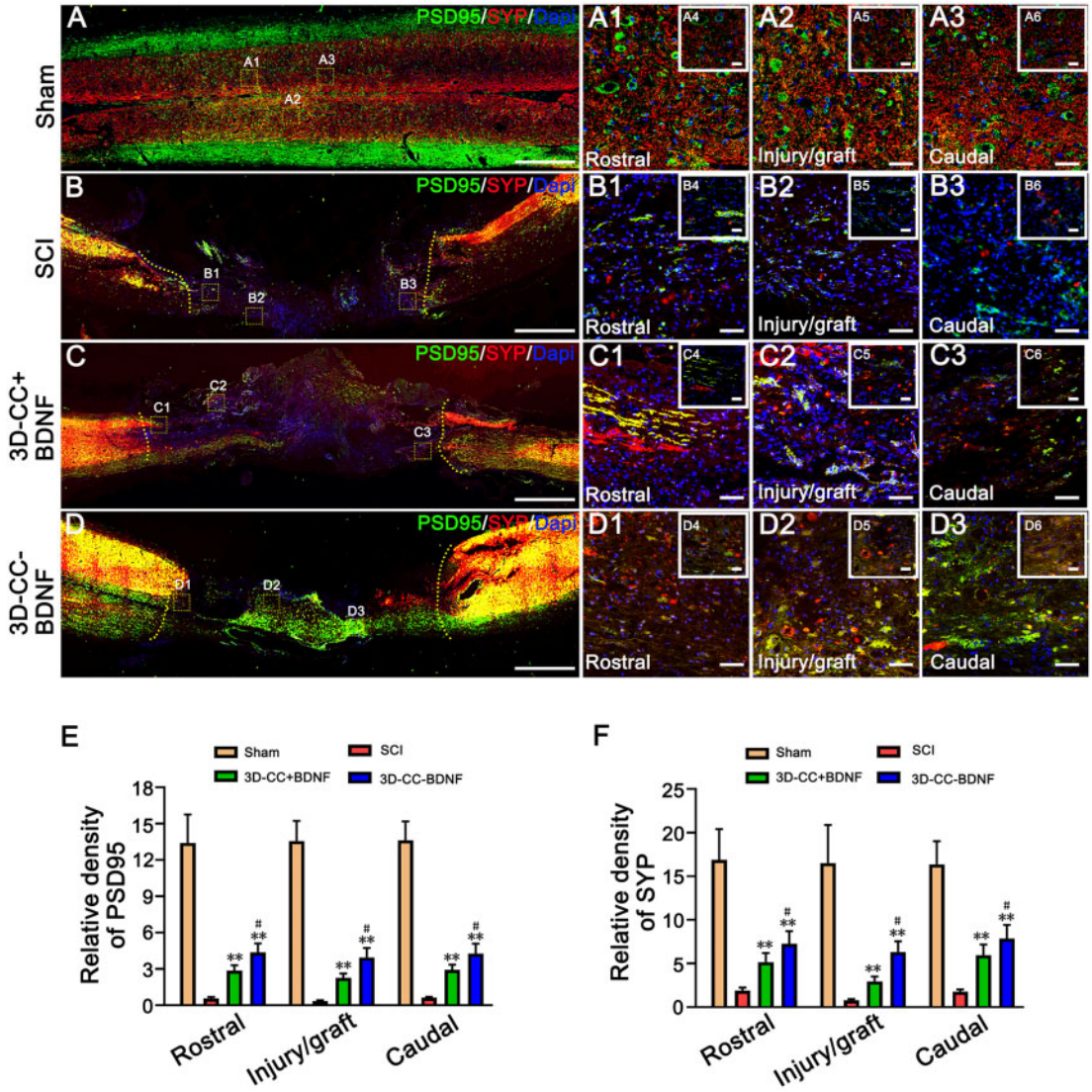

Figure 8. The establishment of synaptic connections at 8 weeks post-surgery. (**A–D**, A1–A3, B1–B3, C1–C3, D1–D3) The typical images of PSD95-positive (green) and SYP-positive (red) synaptic-like structures immunofluorescence staining in longitudinal sections of spinal cord. (A1–A3), (B1–B3), (C1–C3) and (D1-D3) were an amplified image of the yellow box in (A–D), respectively, demonstrating the PSD95-positive staining and SYP-positive staining in the rostral area, the injury/graft site and caudal area of spinal cord. (A4–A6), (B4–B6), (C4–C6) and (D4–D6) were larger magnified images of the yellow box in (A–D). (**E, F**) The quantification of the relative density of PSD95 (E) and SYP (F) in the rostral area, the injury/graft site and caudal area of spinal cord. $^{**}P < 0.01$ vs SCI group. $^{\#}P < 0.05$ vs 3D-CC+BDNF group. Scale bars = 500 μm in panels (A–D), 50 μm in panels (A1–A3, B1–B3, C1–C3, D1–D3), 20 μm in panels (A4–A6, B4–B6, C4–C6, D4–D6). n = number of animals under each condition (n is expressed as dots in the bars). In A–F, $n = 15$.

release more growth factors compared with scaffolds adsorbed with growth factors. Traditional 3D printing technology (such as SLS and 3D powder printing) uses high temperature or chemicals, which damage the biological activity of growth factors during printing [10]. In this study, we overcome these obstacles by low temperature 3D printing. The 3D printing technology was adopted in the printing process to add growth factors in the process of pulp preparation. The printing process was carried out at low temperature to minimize the loss of activity of growth factors. The growth factor utilization rate was high during printing process, and the BDNF was added into the collagen–chitosan compound material, so that the growth factor could be released slowly in the collagen–chitosan compound material. In our study, low temperature 3D printing of collagen/chitosan scaffold integrated with BDNF could maintain the biological activity of BDNF and release more BDNF in a significantly stable manner, thereby promoting the neural regeneration to enable functional recovery compared to 3D printing of collagen/chitosan scaffolds adsorbed with BDNF.

Natural materials can show the advantages of inherent environmental response characteristics through degradation and remodeling compared with synthetic polymers. In recent years, collagen and chitosan materials have been widely used in various tissue engineering and biomedical applications for the advantage of biodegradability, good biocompatibility, low antigenicity and absence of pyrogenic effects [5, 46, 48, 49]. Collagen and chitosan were also selected as materials for 3D printing and promoting nerve regeneration after SCI in this study. BDNF promotes the development of mature nervous systems, maintains neuronal survival and function, and supports differentiation of different neuronal populations [50]. BDNF can also decrease associated injury, ameliorated neurological

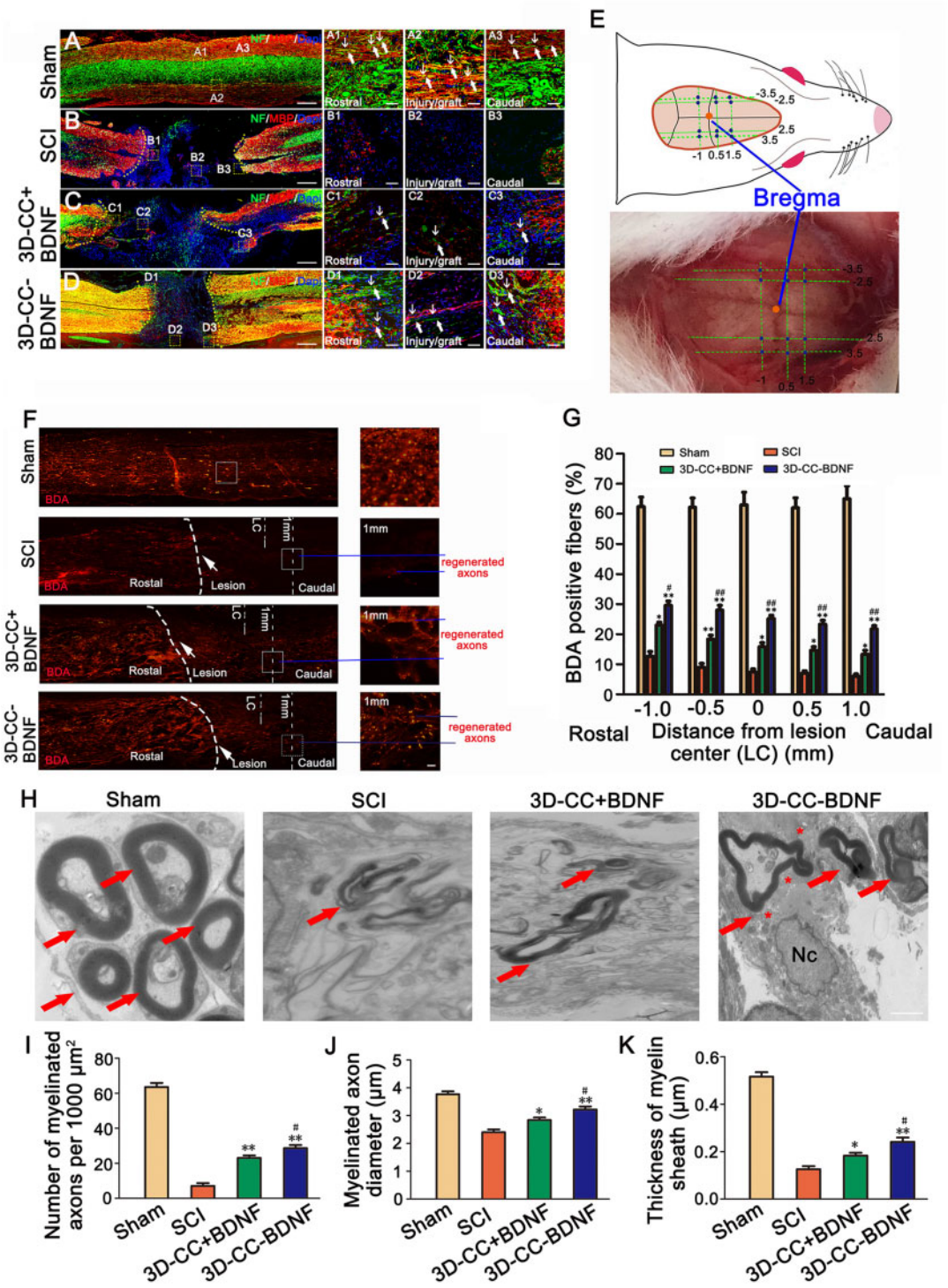

Figure 9. Myelination in the injury/graft site of spinal cord, the results of BDA tracing and the TEM images at the injury site. (**A–D**, A1–A3, B1–B3, C1–C3, D1–D3) The typical images of NF-positive nerve fibers (green, white arrow) and MBP positive myelin-like structures (red, white arrow) immunofluorescence staining in longitudinal sections of spinal cord. (A1–A3), (B1–B3), (C1–C3) and (D1–D3) were an amplified image of the yellow box in (A–D), respectively, demonstrating the NF-positive staining and MBP-positive staining in the rostral area, the injury/graft site and caudal area of spinal cord. (**E**) The image showed the 12 positions of the injection BDA (blue dot) and the position of Bregma (yellow dot). (**F**) The representative images of BDA staining (red) in longitudinal sections of spinal cord. Low magnification (50×) of spinal cord sections (left) and higher magnification (200×) of the white boxed sections (right). The white arrow pointed out the lesion. The blue line indicated the regenerated axons. (**G**) The quantification of BDA positive CST fibers staining at −1 mm, −0.5 mm, 0 mm, 0.5 mm and 1 mm distance caudal to the lesion center. (**H**) Representative transmission electron micrographs at the injury site. All red arrows showed myelinated nerve fibers. All asterisks indicated unmyelinated nerve fibers. Nc = nucleus. (**I–K**) The quantification of the number of myelinated axons (I), myelinated axons diameter (J) and thickness of myelin sheath (K) at the injury site. $^{*}P < 0.05$, $^{**}P < 0.01$ vs SCI group. $^{\#}P < 0.05$, $^{\#\#}P < 0.01$ vs 3D-CC+BDNF group. Scale bars = 500 μm in panels (A–D), 50 μm in panels (A1–A3, B1–B3, C1–C3, D1–D3, F), 1 μm in panel (H). *n* = number of animals under each condition (*n* is expressed as dots in the bars). In A–D, *n* = 15; In E–G, *n* = 5; In H–K, *n* = 5.

function, reduce secondary damage after SCI [51, 52] and stimulate the differentiation of neural stem cells into neurons and oligodendrocytes. The goal of our study is to provide a good microenvironment for spinal cord nerve regeneration by 3D printing of collagen/chitosan scaffolds integrated with BDNF. Our data indicated that 3D printing of collagen/chitosan scaffolds integrated with BDNF increased the bioactivity of BDNF. More importantly, the BDNF release time of 3D-CC-BDNF last up to 28 days. 3D printing could improve the ability of collagen/chitosan to fix BDNF, which created a releasing system for SCI repair.

The mechanical properties of the scaffolds depend not only on the composition but also on the pore structure. Scaffolds prepared by conventional scaffold manufacturing methods (such as freeze drying, organic foam impregnation, particle leaching and so on [53, 54]) are amorphous and irregular, which is difficult to guide axonal regeneration across the injury site. To overcome these difficulties, as an emerging printing technology, 3D printing technology has print orientation, which can meet the requirements of proper shape, size and surface morphology of spinal cord implants [9, 14, 40, 55]. The low temperature 3D printing and freeze-drying technology can accurately construct a tissue engineering scaffold with a combination of macrostructure and microstructure. The principle is that the composite material is made into a porous structure scaffold through the printing device according to the model path, and a large number of micropores are formed after vacuum freeze-drying solvent sublimation. The scaffold is prepared in a low temperature environment, which not only regulates the pore size, porosity and specific surface area of the scaffold, but also helps to maintain the biological activity of raw materials and growth factors, and achieve complementary advantages of the composite materials [56]. In our study, we used a low temperature 3D printer to prepare collagen chitosan-integrated BDNF based on pre-designed structure and size, which could directionally integrate BDNF into collagen chitosan material. The results of light microscopy, SEM and HE staining indicated that the internal structure of 3D-CC-BDNF fabricated by the low temperature 3D printer was regular and porous, which promoted a continuous guiding channel for the regenerated axons and facilitated the exchange of oxygen and nutrients and the adhesion of cells [57]. The mechanical properties of the scaffold are determined by the biomaterial that makes up the scaffold. Compared to the 3D-C-BDNF and 3D-C+BDNF, 3D-CC-BDNF and 3D-CC+BDNF could significantly reduce water absorption, increased porosity and elastic modulus. According to the *in vivo* degradation test of scaffolds, 3D-CC-BDNF scaffold with the mass ratios (collagen:chitosan = 2:1) was an ideal choice for the repair experiment of rat with complete spinal cord transection.

Besides good mechanical properties, the good compatibility of the scaffold is also the key to assessing scaffold biomaterial for the treatment of SCI. Under light microscopy, scanning electron microscopy, HE staining and immunofluorescence staining, we could observe that NSCs or HUCMSCs grew well in 3D-CC-BDNF at 7 days after co-culture. Compared to 3D-CC+BDNF, 3D-CC-BDNF could increase the viability of NSCs or HUCMSCs, which indicated low temperature 3D printing of collagen/chitosan scaffolds integrated with BDNF could release more BDNF to provide a good microenvironment for promoting adhesion, the survival and growth of NSCs or HUCMSCs. To demonstrate the advantages of low temperature 3D printing of scaffolds integrated with growth factor, NSCs were co-cultured with 3D-CC-BDNF and 3D-CC+BDNF. The results showed that 3D-CC-BDNF could significantly augment NeuN cell density and the ratio of NeuN+/Dapi compared to 3D-CC+BDNF, indicating that 3D-CC-BDNF could release more BDNF to promote the survival and maturation of NSCs *in vitro*. The results of *in vivo* release showed that the implantation of 3D-CC-BDNF could prominently increase the BDNF concentration in spinal cord tissue compared to the implantation of 3D-CC+BDNF, suggesting that 3D-CC-BDNF could effectively ameliorate the bioavailability of BDNF. These results proved that the 3D-CC-BDNF had good cytocompatibility.

Functional recovery is the priority of clinical treatment of SCI. In our study, the results of behavioral assessment and electrophysiological studies showed that 3D-CC-BDNF ameliorated locomotor function in rats after SCI. The functional recovery was consistent with the results of MRI, DTI, histological analysis, immunofluorescence staining and BDA. Traditional MRI is considered to be the gold standard imaging model in SCI assessment. However MRI may not be effective or reliable in assessing nerve regeneration after SCI. Our study showed that DTI is a good indicator of SCI in rats. The DTI method can reflect the subtle pathophysiological changes of the injured spinal cord and is regarded as an ideal imaging tool for assessing the extent of recovery after SCI. Although traditional MRI can describe histological changes in the spinal cord [58, 59], most of the data is qualitative. But DTI provides quantitative information about tissue microstructures, such as axons. DTI is an imaging method based on the diffusion of water molecules in tissues. DTI has been shown to be a more sensitive SCI imaging mode than the standard T2WI. As we have reported before, DTI can assess spinal cord integrity and monitor microstructural changes [60]. In the current study, we examined two DTI parameters, consecutive FA and ADC values. The results of DTT can be traced to the local fibers in the lesions of rats with SCI. In this study, we examined the FA and ADC values of the lesion. These two parameters represent different forms. The FA value quantifies SCI severity. In fact, the FA value reflects white matter integrity, including axonal structural damage and demyelination. The decrease in FA value and the increase in ADC reflect neurodegeneration and axonal loss. In our study, the better the damage recovery, the higher the FA value and the lower the ADC value. In contrast, DTI is more sensitive than conventional MRI to detect SCI recovery. The results of MRI and DTI indicated the repair of the 3D-CC-BDNF group was markedly better than the SCI group and the 3D-CC+BDNF group, which suggested that 3D-CC-BDNF could promote the healing of SCI.

Glial scars are usually formed in the injury area after SCI, which inhibits the regeneration of nerve fibers. From the macroscopic histology images and HE staining, it could be seen that the implantation of 3D-CC-BDNF could significantly reduce the formation of tissue cavities and glial scars, promote the regeneration of spinal nerve fibers and the recovery of locomotor function. The results of Bielschowsky's silver staining also indicated that there were more nerve fibers in the injured area of the 3D-CC-BDNF group. These results of histological analysis might explain why the BBB score were increased, the slope angle was increased, the amplitude of MEP and SEP became higher, and the latency were shortened, which indicated the recovery of locomotor function.

In our study, it was found that NF-positive nerve fibers were significantly more in the spinal cord injury area of the 3D-CC-BDNF group, and there were more NF-positive nerve fibers wrapped by MBP positive myelin sheath structures in the injury/graft site of the spinal cord injury area of the 3D-CC-BDNF group. These might be because the 3D-CC-BDNF created a microenvironment that was conducive to nerve fiber regeneration, and the sustained release of BDNF acted as a neurotrophic effect

[61–64]. We found some NF-positive nerve fibers in the injury/graft site of SCI area of the 3D-CC-BDNF group, which demonstrated that 3D-CC-BDNF could guide the growth of NF-positive nerve fibers toward the injury/graft site of the injury area. But we also needed to prove that the regenerated nerve fibers were from the rostral and/or the caudal of SCI area. Through the results of BDA tracing, we believed that regenerated nerve fibers were most likely to come from the rostral of the injury area. At the injury/graft site of the SCI area, we observed that GAP43 immunoreactivity at the injury/graft site in the 3D-CC-BDNF group was significantly more than in the SCI group and the 3D-CC+BDNF group, indicating that implanting the 3D-CC-BDNF could increase axonal regeneration [65]. Axons are the basis for reconstructing neural networks in SCI area for physiological signal transduction [66]. BDNF might induce cortical spinal cord axon growth by activation of TrkB after SCI. Compared to SCI group and 3D-CC+BDNF group, 3D-CC-BDNF group could reduce the accumulation of GFAP-positive glial scar in the injury/graft site of SCI area. The implantation of 3D-CC-BDNF increased the expression of PSD95 and SYP, indicating that more synaptic-like structures were formed in 3D-CC-BDNF group compared to 3D-CC+BDNF. The implantation of 3D-CC-BDNF could increase the number of NF-positive nerve fibers wrapped by MBP positive myelin sheath structures to enhance the regeneration of nerve fibers and myelin sheath at the injury/graft site. Furthermore, transplantation of 3D-CC-BDNF enhanced remyelination at the injury/graft site. These results could indicate that 3D-CC-BDNF could bridge the rostral and caudal of SCI area by creating a microenvironment that was conducive to spinal cord regeneration. The ideal neurotrophic effect in nerve fiber regeneration was attributed to the sustained release of BDNF from the collagen/chitosan scaffolds integrated with BDNF by low temperature extrusion 3D printing. BDA results showed that there were more regenerated CST fibers in the 3D-CC-BDNF group and pass through the cavity at the lesion compare with the SCI group and the 3D-CC+BDNF group [67]. The results of BDA demonstrated that the disrupted nerve fibers in the injury region had a bypass junction, produced new CST fiber and synapses for signal transduction [68]. In general, the scaffolds in our study could increase the content of BDNF in the injury area, which provided more nutrients and created a good microenvironment, to bridge the rostral and caudal of SCI area and to enable functional recovery.

Conclusions

In this study, the collagen/chitosan scaffolds integrated with BDNF by low temperature extrusion 3D printing exhibited good biological activity and biocompatibility *in vitro*. We found that low temperature extrusion 3D printing preserved the biological activity of BDNF. Compared to 3D printed collagen/chitosan scaffolds adsorbed with brain-derived neurotrophic factor (3D-CC+BDNF), collagen/chitosan scaffolds integrated with brain-derived neurotrophic factor (3D-CC-BDNF) by low temperature extrusion 3D printing released more BDNF continuously, which could provide more cell binding sites and further promoted adhesion and proliferation of NSCs and HUCMSCs. When 3D-CC-BDNF prepared by low temperature extrusion 3D printing were transplanted into the injury site in a complete spinal cord transection rat model, the presence of BDNF could further promote the neural regeneration, reduce cavity and glial scars formation at the injury site. Correspondingly, the transplantation of 3D-CC-BDNF could further significantly ameliorated the locomotor function. Transplantation of 3D-CC-BDNF at the injury site could be a potential therapeutic method for clinical treatment of SCI.

Supplementary data

supplementary materials are available at *REGBIO* online.

Acknowledgments

This work was supported by the National Nature Scientific Fund of China (81771352, 81971782, 81771350) and the Nature Scientific Fund of Tianjin (18JCJQJC48500, 19JCYBJC27900).

Conflict of interest statement. None declared.

References

1. Devivo MJ, Krause JS, Lammertse DP. Recent trends in mortality and causes of death among persons with spinal cord injury. *Arch Phys Med Rehabil* 1999;**80**:1411–9.
2. Nilsson BP, Nilsson JA. Mechanisms of axonal dysfunction after spinal cord injury: with an emphasis on the role of voltage-gated potassium channels. *Brain Res Rev* 2001;**38**:165–91.
3. Wright KT, El MW, Osman A *et al.* Concise review: bone marrow for the treatment of spinal cord injury: mechanisms and clinical applications. *Stem Cells* 2011;**29**:169–78.
4. Altinova H, Hammes S, Palm M *et al.* Fibroadhesive scarring of grafted collagen scaffolds interferes with implant-host neural tissue integration and bridging in experimental spinal cord injury. *Regen Biomater* 2019;**6**:75–87.
5. Zhang L, Fan C, Hao W *et al.* NSCs migration promoted and drug delivered exosomes-collagen scaffold via a bio-specific peptide for one-step spinal cord injury repair. *Adv Healthc Mater* 2021;**10**:e2001896.
6. Li L, Zhang Y, Mu J *et al.* Transplantation of human mesenchymal stem-cell-derived exosomes immobilized in an adhesive hydrogel for effective treatment of spinal cord injury. *Nano Lett* 2020;**20**:4298–305.
7. Li G, Che MT, Zhang K *et al.* Graft of the NT-3 persistent delivery gelatin sponge scaffold promotes axon regeneration, attenuates inflammation, and induces cell migration in rat and canine with spinal cord injury. *Biomaterials* 2016;**83**:233–48.
8. Ogier M, Kron M, Katz DM. Neurotrophic factors in development and regulation of respiratory control. *Compr Physiol* 2013;**3**:1125–34.
9. Inzana JA, Olvera D, Fuller SM *et al.* 3D printing of composite calcium phosphate and collagen scaffolds for bone regeneration. *Biomaterials* 2014;**35**:4026–34.
10. Kelder C, Bakker AD, Klein-Nulend J *et al.* The 3D printing of calcium phosphate with K-Carrageenan under conditions permitting the incorporation of biological components-A method. *J Funct Biomater* 2018;**9**:57.
11. Schubert C, van Langeveld MC, Donoso LA. Innovations in 3D printing: a 3D overview from optics to organs. *Br J Ophthalmol* 2014;**98**:159–61.
12. Wong DY, Leveque JC, Brumblay H *et al.* Macro-architectures in spinal cord scaffold implants influence regeneration. *J Neurotrauma* 2008;**25**:1027–37.
13. Sun Y, Yang C, Zhu X *et al.* 3D printing collagen/chitosan scaffold ameliorated axon regeneration and neurological recovery after spinal cord injury. *J Biomed Mater Res A* 2019;**107**:1898–908.
14. Tan Y, Richards DJ, Trusk TC *et al.* 3D printing facilitated scaffold-free tissue unit fabrication. *Biofabrication* 2014;**6**:024111.
15. Koffler J, Zhu W, Qu X *et al.* Biomimetic 3D-printed scaffolds for spinal cord injury repair. *Nat Med* 2019;**25**:263–9.
16. Choi E, Kim D, Kang D *et al.* 3D-printed gelatin methacrylate (GelMA)/silanated silica scaffold assisted by two-stage cooling system for hard tissue regeneration. *Regen Biomater* 2021;**8**:rbab001.
17. Liu X, Hao M, Chen Z *et al.* 3D bioprinted neural tissue constructs for spinal cord injury repair. *Biomaterials* 2021;**272**:120771.

18. Xu T, Jin J, Gregory C *et al.* Inkjet printing of viable mammalian cells. *Biomaterials* 2005;**26**:93–9.
19. Seol YJ, Kang HW, Lee SJ *et al.* Bioprinting technology and its applications. *Eur J Cardiothorac Surg* 2014;**46**:342–8.
20. Richard RC, Sader MS, Dai J *et al.* Beta-type calcium phosphates with and without magnesium: from hydrolysis of brushite powder to robocasting of periodic scaffolds. *J Biomed Mater Res A* 2014;**102**:3685–92.
21. Garvin J, Qi J, Maloney M *et al.* Novel system for engineering bioartificial tendons and application of mechanical load. *Tissue Eng* 2003;**9**:967–79.
22. Group EBCTC. Effects of chemotherapy and hormonal therapy for early breast cancer on recurrence and 15-year survival: an overview of the randomised trials. *Lancet* 2005;**365**:1687–717.
23. Rao SB, Sharma CP. Use of chitosan as a biomaterial: studies on its safety and hemostatic potential. *J Biomed Mater Res* 1997;**34**:21–8.
24. Fei-Xiang Y, Ai-Feng Z, Peng H *et al.* Effect of neurotrophin 3- chitosan on endogenous neurogenesis and motor function after motor cortex injury in rats. *Chinese J Rehabil Theory Pract* 2017;**12**:155–161.
25. He X, Yang X, Jabbari E. Combined effect of osteopontin and BMP-2 derived peptides grafted to an adhesive hydrogel on osteogenic and vasculogenic differentiation of marrow stromal cells. *Langmuir* 2012;**28**:5387–97.
26. Keefe KM, Sheikh IS, Smith GM. Targeting neurotrophins to specific populations of neurons: NGF, BDNF, and NT-3 and their relevance for treatment of spinal cord injury. *Int J Mol Sci* 2017;**18**:548.
27. Liang W, Han Q, Jin W *et al.* The promotion of neurological recovery in the rat spinal cord crushed injury model by collagen-binding BDNF. *Biomaterials* 2010;**31**:8634–41.
28. Liang J, Deng G, Huang H. The activation of BDNF reduced inflammation in a spinal cord injury model by TrkB/p38 MAPK signaling. *Exp Ther Med* 2019;**17**:1688–96.
29. Fouad K, Vavrek R, Cho S. A TrkB antibody agonist promotes plasticity after cervical spinal cord injury in adult rats. *J Neurotrauma* 2021;**38**: 1338–48.
30. Ye JH, Houle JD. Treatment of the chronically injured spinal cord with neurotrophic factors can promote axonal regeneration from supraspinal neurons. *Exp Neurol* 1997;**143**:70–81.
31. Liu XY, Liang J, Wang Y *et al.* Diffusion tensor imaging predicting neurological repair of spinal cord injury with transplanting collagen/chitosan scaffold binding bFGF. *J Mater Sci Mater Med* 2019;**30**:123.
32. Song Y, Lin K, He S *et al.* Nano-biphasic calcium phosphate/polyvinyl alcohol composites with enhanced bioactivity for bone repair via low-temperature three-dimensional printing and loading with platelet-rich fibrin. *Int J Nanomedicine* 2018;**13**:505–23.
33. Jiang J, Liu X, Chen H *et al.* 3D printing collagen/heparin sulfate scaffolds boost neural network reconstruction and motor function recovery after traumatic brain injury in canine. *Biomater Sci* 2020;**8**:6362–74.
34. Zeng S, Liu L, Shi Y *et al.* Characterization of silk fibroin/chitosan 3D porous scaffold and in vitro cytology. *PLoS One* 2015;**10**:e0128658.
35. Sarikaya B, Aydin HM. Collagen/beta-tricalcium phosphate based synthetic bone grafts via dehydrothermal processing. *Biomed Res Int* 2015; **2015**:576532.
36. Harris J, Lee H, Tu CT *et al.* Preparing e18 cortical rat neurons for compartmentalization in a microfluidic device. *J Vis Exp* 2007;**8**:305.
37. Liu XY, Wei MG, Liang J *et al.* Injury-preconditioning secretome of UCMSCs amplified the neurogenesis and cognitive recovery after severe traumatic brain injury in rats. *J Neurochem* 2020;**153**:230–51.
38. Tu Y, Chen C, Sun HT *et al.* Combination of temperature-sensitive stem cells and mild hypothermia: a new potential therapy for severe traumatic brain injury. *J Neurotrauma* 2012;**29**:2393–403.
39. Liu XY, Wei MG, Liang J *et al.* Injury-preconditioning secretome of umbilical cord mesenchymal stem cells amplified the neurogenesis and cognitive recovery after severe traumatic brain injury in rats. *J Neurochem* 2020;**153**:230–51.
40. Chen C, Zhao ML, Zhang RK *et al.* Collagen/heparin sulfate scaffolds fabricated by a 3D bioprinter improved mechanical properties and neurological function after spinal cord injury in rats. *J Biomed Mater Res A* 2017;**105**:1324–32.
41. Chen X, Zhao Y, Li X *et al.* Functional multichannel poly(propylene fumarate)-collagen scaffold with collagen-binding neurotrophic factor 3 promotes neural regeneration after transected spinal cord injury. *Adv Healthc Mater* 2018;**7**:e1800315.
42. Cai Z, Gan Y, Bao C *et al.* Photosensitive hydrogel creates favorable biologic niches to promote spinal cord injury repair. *Adv Healthc Mater* 2019;**8**:e1900013.
43. Zeng X, Zeng YS, Ma YH *et al.* Bone marrow mesenchymal stem cells in a three-dimensional gelatin sponge scaffold attenuate inflammation, promote angiogenesis, and reduce cavity formation in experimental spinal cord injury. *Cell Transplant* 2011;**20**:1881–99.
44. Yao S, Yu S, Cao Z *et al.* Hierarchically aligned fibrin nanofiber hydrogel accelerated axonal regrowth and locomotor function recovery in rat spinal cord injury. *Int J Nanomedicine* 2018;**13**:2883–95.
45. Loh QL, Choong C. Three-dimensional scaffolds for tissue engineering applications: role of porosity and pore size. *Tissue Eng Part B Rev* 2013; **19**:485–502.
46. Yang Z, Zhang A, Duan H *et al.* NT3-chitosan elicits robust endogenous neurogenesis to enable functional recovery after spinal cord injury. *Proc Natl Acad Sci U S A* 2015;**112**:13354–9.
47. Fan C, Li X, Zhao Y *et al.* Cetuximab and Taxol co-modified collagen scaffolds show combination effects for the repair of acute spinal cord injury. *Biomater Sci* 2018;**6**:1723–34.
48. Pires LR, Pêgo AP. Bridging the lesion-engineering a permissive substrate for nerve regeneration. *Regen Biomater* 2015;**2**:203–14.
49. Tian L, Prabhakaran MP, Ramakrishna S. Strategies for regeneration of components of nervous system: scaffolds, cells and biomolecules. *Regen Biomater* 2015;**2**:31–45.
50. Hempstead BL. Brain-derived neurotrophic factor: three ligands, many actions. *Trans Am Clin Climatol Assoc* 2015;**126**:9–19.
51. Baker-Herman TL, Fuller DD, Bavis RW *et al.* BDNF is necessary and sufficient for spinal respiratory plasticity following intermittent hypoxia. *Nat Neurosci* 2004;**7**:48–55.
52. Kamei N, Tanaka N, Oishi Y *et al.* BDNF, NT-3, and NGF released from transplanted neural progenitor cells promote corticospinal axon growth in organotypic cocultures. *Spine (Phila Pa 1976)* 2007;**32**:1272–8.
53. Evans GR, Brandt K, Niederbichler AD *et al.* Clinical long-term in vivo evaluation of poly(L-lactic acid) porous conduits for peripheral nerve regeneration. *J Biomater Sci Polym Ed* 2000;**11**:869–78.
54. Maquet V, Martin D, Scholtes F *et al.* Poly(D,L-lactide) foams modified by poly(ethylene oxide)-block-poly(D,L-lactide) copolymers and a-FGF: in vitro and in vivo evaluation for spinal cord regeneration. *Biomaterials* 2001;**22**:1137–46.
55. Rosenzweig DH, Carelli E, Steffen T *et al.* 3D-printed ABS and PLA scaffolds for cartilage and nucleus pulposus tissue regeneration. *Int J Mol Sci* 2015;**16**:15118–35.
56. Domingos M, Intranuovo F, Gloria A *et al.* Improved osteoblast cell affinity on plasma-modified 3-D extruded PCL scaffolds. *Acta Biomater* 2013; **9**:5997–6005.
57. Reynolds LF, Bren MC, Wilson BC *et al.* Transplantation of porous tubes following spinal cord transection improves hindlimb function in the rat. *Spinal Cord* 2008;**46**:58–64.
58. Huang SL, He XJ, Xiang L *et al.* CT and MRI features of patients with diastematomyelia. *Spinal Cord* 2014;**52**:689–92.
59. Huang SL, Liu YX, Yuan GL *et al.* Characteristics of lumbar disc herniation with exacerbation of presentation due to spinal manipulative therapy. *Medicine (Baltimore)*. 2015;**94**:e661.
60. Wang F, Huang SL, He XJ *et al.* Determination of the ideal rat model for spinal cord injury by diffusion tensor imaging. *Neuroreport* 2014; **25**:1386–92.
61. Bradbury EJ, Khemani S, Von R *et al.* NT-3 promotes growth of lesioned adult rat sensory axons ascending in the dorsal columns of the spinal cord. *Eur J Neurosci* 2010;**11**:3873–83.

62. Schnell L, Schneider R, Kolbeck R *et al.* Neurotrophin-3 enhances sprouting of corticospinal tract during development and after adult spinal cord lesion. *Nature* 1994;**367**:170–3.
63. Taylor SJ, McDonald JW, Sakiyama-Elbert SE. Controlled release of neurotrophin-3 from fibrin gels for spinal cord injury. *J Control Release* 2004;**98**:281–94.
64. Xu XM, Guénard V, Kleitman N *et al.* A combination of BDNF and NT-3 promotes supraspinal axonal regeneration into Schwann cell grafts in adult rat thoracic spinal cord. *Exp Neurol* 1995;**134**:261–72.
65. Zhou Z, Chen Y, Zhang H *et al.* Comparison of mesenchymal stromal cells from human bone marrow and adipose tissue for the treatment of spinal cord injury. *Cytotherapy* 2013;**15**:434–48.
66. Tang S, Liao X, Shi B *et al.* The effects of controlled release of neurotrophin-3 from PCLA scaffolds on the survival and neuronal differentiation of transplanted neural stem cells in a rat spinal cord injury model. *PLoS One* 2014;**9**:e107517.
67. Liu Y, Ban DX, Ma C *et al.* Photodynamic therapy mediated by upconversion nanoparticles to reduce glial scar formation and promote hindlimb functional recovery after spinal cord injury in rats. *J Biomed Nanotechnol* 2016;**12**:2063–75.
68. Liu J, Chen J, Liu B *et al.* Acellular spinal cord scaffold seeded with mesenchymal stem cells promotes long-distance axon regeneration and functional recovery in spinal cord injured rats. *J Neurol Sci* 2013;**325**:127–36.